Terahertz Holography for Non-line of Sight Imaging

by

Sai Kiran Doddalla

A Thesis Presented in the Partial Fulfillment
of the Requirements for the Degree
Master of Science

Approved August 2019 by the
Graduate Supervisory Committee:

George Trichopoulos, Chair
Ahmed Alkhateeb
Saeed Zeinolabedinzadeh
James Aberle

ARIZONA STATE UNIVERSITY

December 2019

ABSTRACT

The objective of this work is to design a novel method for imaging targets and scenes which are not directly visible to the observer. The unique scattering properties of terahertz (THz) waves can turn most building surfaces into mirrors, thus allowing someone to see around corners and various occlusions. In the visible regime, most surfaces are very rough compared to the wavelength. As a result, the spatial coherency of reflected signals is lost, and the geometry of the objects where the light bounced on cannot be retrieved. Interestingly, the roughness of most surfaces is comparable to the wavelengths at lower frequencies (100 GHz – 10 THz) without significantly disturbing the wavefront of the scattered signals, behaving approximately as mirrors. Additionally, this electrically small roughness is beneficial because it can be used by the THz imaging system to locate the pose (location and orientation) of the mirror surfaces, thus enabling the reconstruction of both line-of-sight (LoS) and non-line-of-sight (NLoS) objects.

Back-propagation imaging methods are modified to reconstruct the image of the 2-D scenario (range, cross-range). The reflected signal from the target is collected using a SAR (Synthetic Aperture Radar) set-up in a lab environment. This imaging technique is verified using both full-wave 3-D numerical analysis models and lab experiments.

The novel imaging approach of non-line-of-sight-imaging could enable novel applications in rescue and surveillance missions, highly accurate localization methods, and improve channel estimation in mmWave and sub-mmWave wireless communication systems.

TABLE OF CONTENTS

Page

CHAPTER Page

Page

LIST OF FIGURES

Figure Page

Figure Page

Figure Page

1 INTRODUCTION

1.1 LoS and NLoS Imaging:

In line-of-sight (LoS) imaging, the object or schene is directly visible from the imaging system, as depicted in Fig 1-1. In Coherent microwave imaging, the transceiver plane is the active imaging aperture, which illuminates the scene with radio-frequency (RF) signals and records the scattered wave-fronts on the imaging plane. Scattered wave amplitude and phase depend on the material and geometry of the target area.

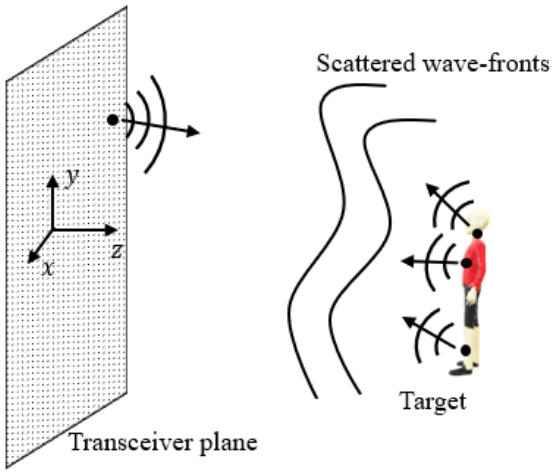

Figure 1-1 Line-of-sight imaging scenario in which transceivers arranged on a plane are used to illuminate and record RF waves.

In Non-line-of-sight (NLoS) imaging, the object is not directly visible due to an occlusion that restricts the direct backscattering to the imaging aperture. Hence, image reconstruction depends on the waves scattered from a surrounding surface[1]-[2], as shown in Figure 1-2. Here, the emitted radiation is first bounced off a neighboring surface (open door), which

then bounces off the target before it propagates back to the imaging system. NLoS is a potential application for autonomous driving, surveillance, and other applications, which will be briefly discussed in further sections.

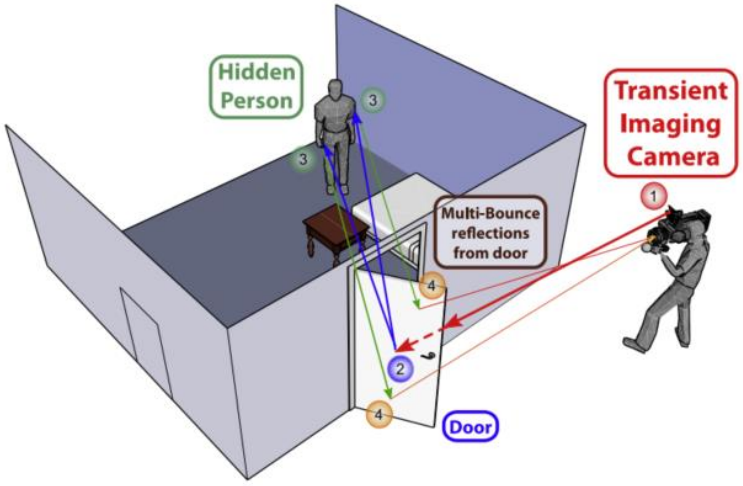

Figure 1-2 Illustrates the NLoS imaging scenario. Here is a contrast to the above figure a man is scanned based on the multi bounce from the door[1]

1.2 Holography the Basis of 3-D Imaging:

Holography is an optical technique that is developed to form 3-D images on a 2-D surface by illuminating the object with a coherent light source [3]-[4]. A coherent light source corresponds to an optical wave with a single frequency component. Holography is based upon wavefront sampling and reconstruction. The concept of holography was first invented and demonstrated by Dennis Gabor in 1948, but his work was recognized and awarded with a Noble 20 years later, in 1971 [3].

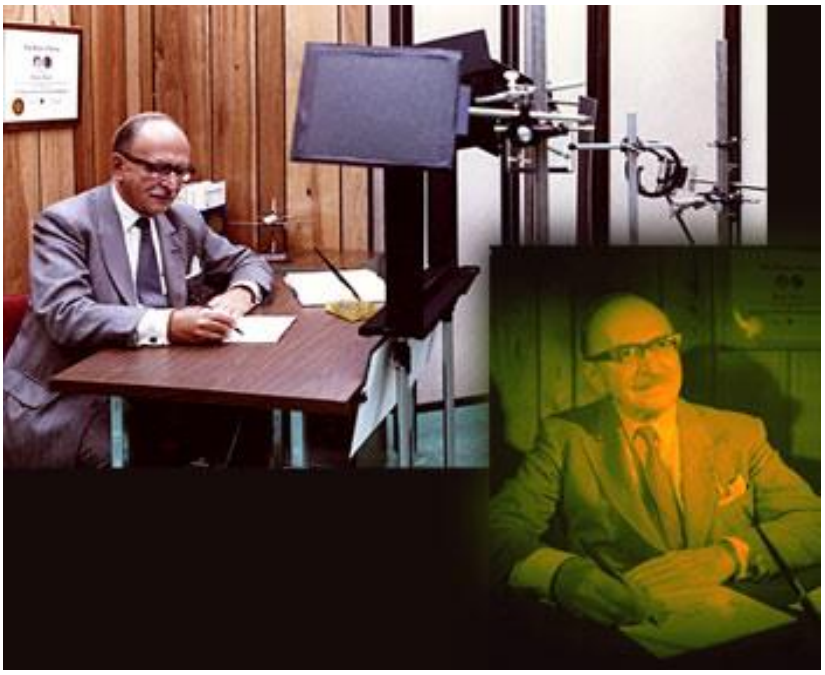

Figure 1-3 Dennis Gabor demonstrating holography with his hologram placed at the corner (Source:nobleprize.org)

Gabor was trying to improve the resolution of a microscope by using holography, and he observed that every object exhibits a unique wave-interference pattern when excited with a coherent beam. Figure 1-3 shows the lab demonstration of holography created by Dennis Gabor. However, this concept came to practical existence with the invention of the laser. The laser is not only a highly coherent beam but also has a strong intensity, making holography possible. The first step in holography is shown in Figure 1-4, where an object that is to be imaged is illuminated using a coherent beam to form a unique interference pattern. The unique wave-fronts from the object are combined with the reference beam to form a crest and trough pattern of the object. The amplitude and phase of this coherent wave interference pattern are later recorded on a photographic plate.

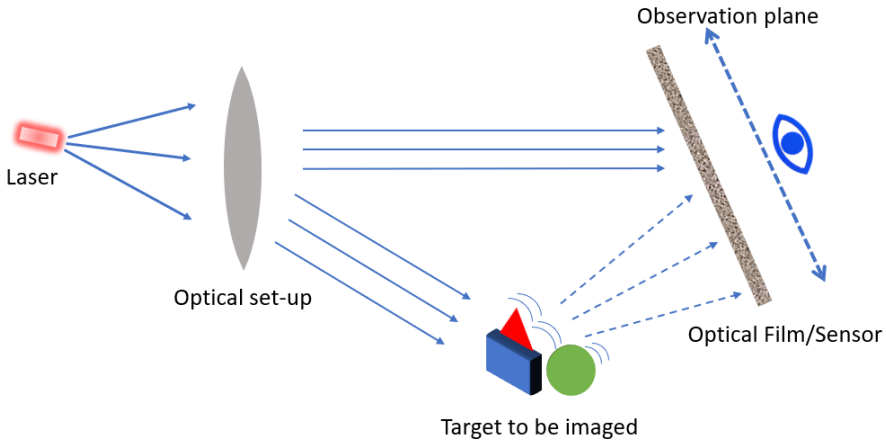

Figure 1-4 Optical set-up for storing the hologram of the objects on to a film. Optical set-up corresponds to beam splitters and other lenses to focus the coherent beam.

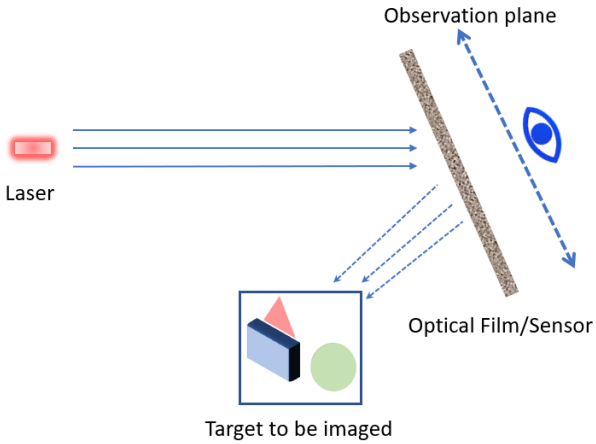

Figure 1-5 The reference beam is focused on the optical film to create the 3-D image of objects. Looking from a different position on the observation plane exposes the different perspectives of the object.

The unique interference pattern is later used in the second step to display the object onto a screen, as illustrated in Figure 1-5. When the photographic plate is illuminated by a coherent source, the fine, coarse detailed interference fringes on the plate act as a

diffraction grating, the hologram must be illuminated with the same reference beam, i.e., the reference beam direction and distance must be the same as before to reconstruct the object. The light projected onto a screen is placed at the same angle as the illuminated object to form the image, and viewing this image from different points on a 2-D surface exposes the object to different perspectives.

Holography acts as a base for all the photographic equipment that man has invented so far. Reconstruction algorithms, including range migration and phase shift migration algorithms, are based on holography. In these imaging techniques, a reference signal (local oscillator, LO) is routed through high-frequency circuits and mixed with the signals backscattered from the object under imaging. The complex output signal from the mixing of the two signals (LO and backscattered) is used to reconstruct the image. As such, holography can enable low-profile, lensless imaging methods without the use of bulky and heavy focusing elements. This is particularly crucial in the THz regime, where the size of optics can be many orders larger than those of visible light for comparable image resolution.

1.3 Basics of RADAR:

While the holography saw its share of development using optical frequencies, it's equivalent; microwave imaging systems were under progress. Even though the resolution was degraded compared to the optical imaging, microwave systems had their own set of applications and ease of applicability. Using the return signal's amplitude and phase to reconstruct co-ordinates of the object using microwave frequency signals is called RADAR(Radio Detection and Ranging). The name RADAR was first coined by

Hulmseyer in 1901, who used the technology to detect ships. Marconi worked on the development of technology, but it was later in 1920 that RADAR became popular. Detection of man-made objects, weather monitoring, and ground mapping are some of the early applications of RADAR. Later on, concepts of RADAR were used not only to find the positions of the object but also to image the objects in 3-D. Different RADAR technologies, geometries, and capabilities are discussed in the next section.

1.3.1 Properties of RADAR Systems:

Spatial resolution and computational efficiency are the two important metrics of any RADAR system. While the resolution is about the ability of RADAR to separate the smallest targets from each other, the latter is about the computational efficiency of the RADAR algorithm [5]-[6]. Brief points on the resolution are mentioned in this section, while the computational burden of imaging algorithms is dealt with in the next chapter. The temporal resolution depends on the bandwidth or the pulse width of the transmitted signal. Narrow pulse width, though, offers high spatial resolution but has the disadvantage of lower power and hence lower Signal to noise ratio(SNR) of the backscattered signal compared to the receiver-generated noise [5]. FMCW (Frequency modulated continuous wave RADAR) has the advantage of both high bandwidth and longer pulse duration by using the frequency coded pulse called the chirp signal. In an FMCW chirp, each frequency component is time-coded, and hence the difference between the frequency of the Tx pulse and Rx pulse is converted to a distance [7]-[9]. FMCW RADAR is also used to detect the doppler of the moving objects. Stepped frequency RADAR has the same resolution capabilities of an FMCW RADAR, but instead of a frequency-modulated pulse, it uses

discrete frequency sinusoidal waves and combines the response using Fourier transform algorithms. FMCW waves are more suitable for practical RADAR implementation and are a standard for many industrial applications[9]. A VNA(Vector Network Analyzer) can be used to produce a simple sinusoidal signal across the whole bandwidth and collect the scattering parameter data, and hence stepped frequency approach can be easily implemented in a microwave lab.

The angular resolution of the RADAR, i.e., the lowest object dimension that it can detect in the lateral domain or cross-range, can depend on the aperture size of the radar or the beamwidth of the RADAR. Real aperture RADAR scans the whole target area using large-format phased array antenna systems, as shown in Figure 1-6. Larger array dimensions with multiple Tx and Rx antenna elements correspond to narrow beamwidth and hence, better angular capabilities of the radar.

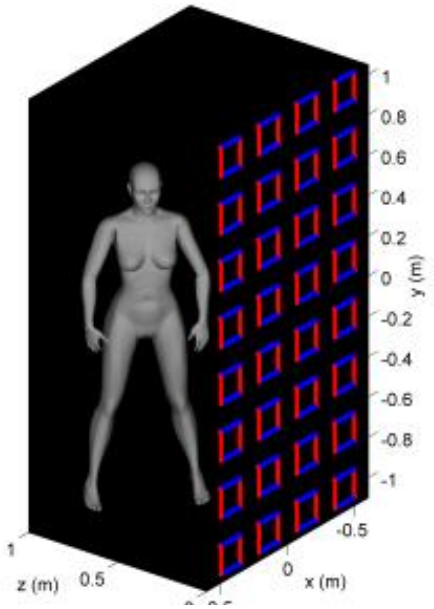

Figure 1-6 Real aperture of antenna elements scanning the entire human being [10]

However, having the largest aperture does not always suffice for various application environments where there are space constraints on RADAR, or the target area is very large(miles), as shown in Figure 1-7. To solve this problem of large aperture Synthetic Aperture RADAR (SAR) systems were proposed. SAR uses a mobile real aperture radar to scan a significant target area. SAR systems record the signal over the whole scanning aperture and then use spatial correlation to map the target data. SAR system was first deployed in 1950 for air observation. Later, the advancements in the field of computing made SAR ubiquitous in surveillance, monitoring, and imaging applications. The resolution of the SAR image depends on the number of antenna positions, the distance between the adjacent scans, and the distance to the target. A simple illustration of a satellite scanning the earth using SAR is given in Figure 1-7.

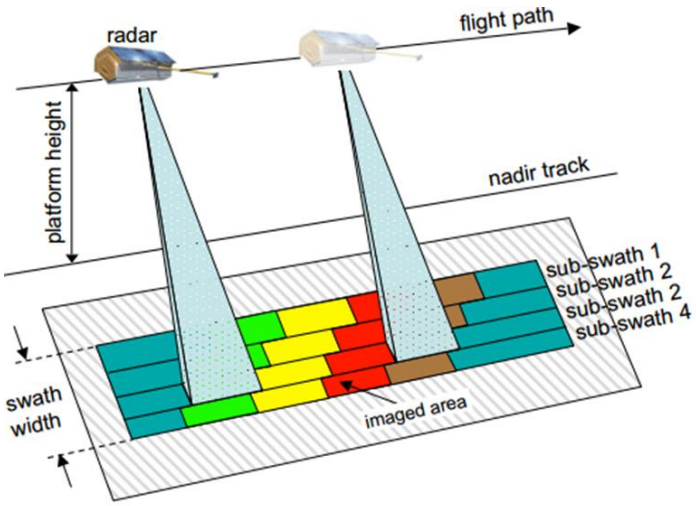

Figure 1-7 Satellite scanning earth one area after another providing the complete land surveillance [11]

1.3.2 Different RADAR Geometries:

RADAR geometry means the spatial arrangement of Tx and RX's to obtain the complete SAR image, as shown in [5],[6]. Different RADAR geometries lead to different resolution and computational properties. Most of the SAR systems are monostatic, but they have mechanical scanning restrictions and a single viewpoint. Monostatic systems provide good resolution but tend to form a ghost object in a complex geometry scenario because they look only at a single point of view of the target. Hence complex imaging systems like bistatic and multistatic were later introduced to achieve better images of complex geometries[12],[13]. In bi-static systems, the transmitter and receiver are separated by a significant distance to achieve better resolutions. Multi-static systems comprise of various spatially diversified mono or bi-static systems. Here in Figure 1-8c of the multi-static system, the additional angular observations made in contrast to mono-static imaging in Figure 1-8(a) creates the possibility of better resolution and ghost-free RADAR images. These systems have different applications based on the resolution required and the complexity of the object geometry under scan. Both bi and multi-static imaging systems are hard to install and computationally demanding and hence only used for applications where higher resolution is required. For example, bistatic imaging is used to map the ionosphere [14] in weather monitoring, and multistatic imaging systems are actively used in short-range imaging applications like security scanning.

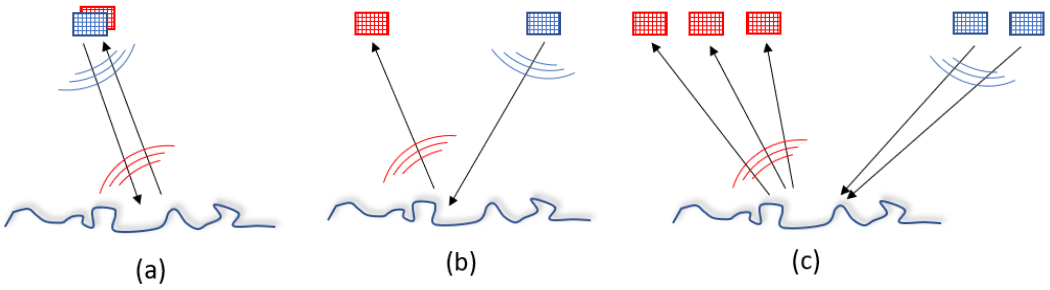

Figure 1-8 Geometries for different RADAR topologies, here blue represents a transmitter and red represents a receiver a) In monostatic topologies, the transmitter and receiver are located in the same point b) In bistatic RADAR geometry, Tx and Rx are separated position c) Generic Multistatic case with 2 Tx and 3Rx.

In the next section, the concept and prior work of NLoSimaging are presented. Discussion on the suitability of THz waves for NLoS technology is given with practical limitations. THz waves prominence in the area of imaging with applications that are best suited to this spectrum is highlighted.

1.4 THz spectrum for Imaging:

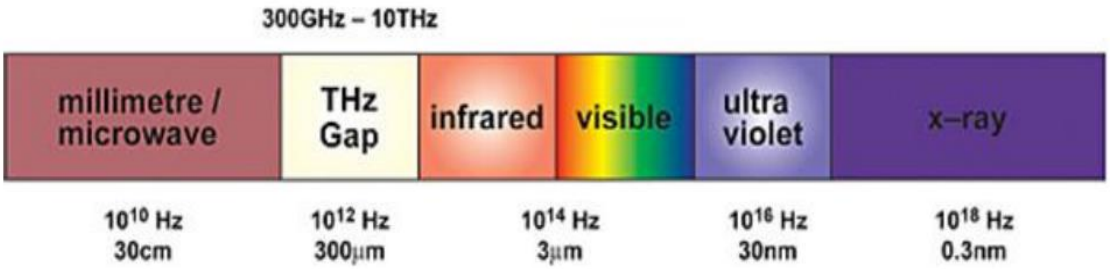

Figure 1-9 THz Gap in the EM spectrum existing between microwave and optical regions[14]

A favorable property is that in contrast to microwave frequencies is that most building surfaces are opaque in the THz spectrum, and surface roughness and material inhomogeneity are comparable to THz wavelengths resulting in diffuse scattering. In an active imaging system, such surfaces can be imaged by recording the THz backscattered signals.

Apart from their favorable scattering properties, THz waves are also attractive for imaging purposes due to their high spatial resolution enabled by short wavelengths and large bandwidths. THz waves can provide centimeter-level image resolution while maintaining low-profile, portable imaging hardware. THz imaging has already been performed in long-range, line-of-sight (LOS) imaging. Such systems have achieved imaging at distances longer than 60 m, and with the development of more powerful sources [15]-[16] the range could increase dramatically. Additionally, due to the short wavelengths, THz imaging systems can achieve reasonable spatial resolution using apertures of practical dimensions. For example, a D = 20 cm diameter aperture system produces an angular resolution of $\theta = \lambda/D$ = 0.18 degrees at 500 GHz, whereas the human eye has a comparable resolution of ~ 0.06 degree.

Penetration capability of THz waves can also be beneficial in low visibility conditions (e.g., fog, smoke), where visible or infrared systems are blind. Nevertheless, THz image quality can vary significantly from the ambient visible light images due to strong speckles that can saturate the image. With the use of proper mitigation methods[17], image distortion can be reduced in LoS THz images. Using wideband signals (depth information) [18], this deleterious effect of speckles can be reduced further. As such, combining the attractive

propagation and *scattering* properties of THz waves in a multireflection scenario, we can acquire adequate information to image hidden scenes.

These modern developments made the RADAR at Terahertz to be a viable technology for imaging systems. Imaging system trends that were talked have been used for many applications in our day to day life. In the next section, some of the applications of these technologies were discussed.

1.5 Spectrum for NLoS Technology:

Visible and infrared light have very short wavelengths, and unless the surface is carefully polished, the light is scattered almost isotropically (diffuse scattering), resulting in image ambiguity. The uneven surface topography results in the wave reflecting with the arbitrary phase at every point on the surface; thus, all the information on the direction of reflected waves is lost, causing ambiguity in the imaging process. Several approaches have been proposed to solve the problem of diffusion, including the use of beam-scanning, picosecond lasers and ultrafast, time-resolving cameras [1]-[2]. Other approaches have simplified the problem by assuming a memory effect of the reflective surfaces [19]-[21]. More straightforward, single beam methods have also been investigated; however, they offer limited imaging capabilities and act mostly as a tracking method [22]-[23]. In general, the practical deployment of visible light systems is still not evolved due to weakly scattered signals, small field of view, and long integration times.

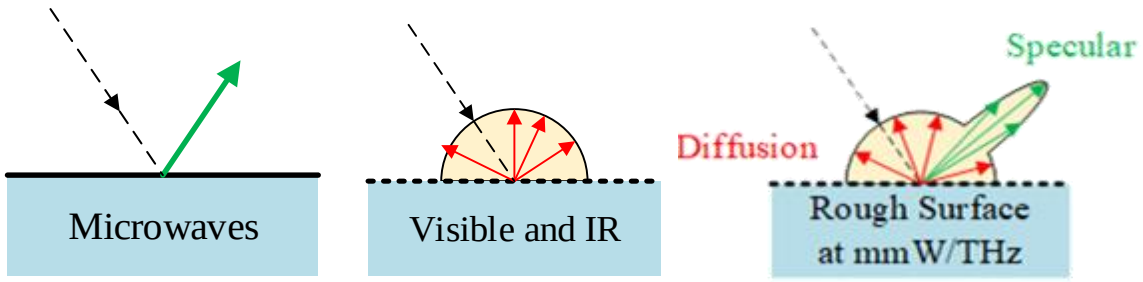

Figure 1-10 (a) Strong specular component due to the scattering of EM waves at the microwave region. (b) Due to the short wavelength of the visible spectrum, the EM energy is scattered almost isotropically. (c) Terahertz's rough surface scattering exhibits both a diffusion and a strong specular component.

Alternatively, lower frequency NLoS radar systems have been investigated. At microwave frequencies, the surface roughness is much smaller than the wavelength. However, in the lower frequency spectrum materials are semitransparent, edge diffractions become stronger, and images are cluttered due to strong multireflection propagation **Error! R eference source not found.-Error! Reference source not found.**. Additionally, radar systems require accurate knowledge of the static geometry and are limited to object detection rather than generating detailed images of the hidden scene.

The proposed work aims at providing solutions to the weaknesses of current NLoS imaging approaches. The unique scattering properties and wide bandwidth of THz signals will allow the proliferation of active imaging systems that can 1) image hidden objects without a priori knowledge of the environment, 2) achieve sub-centimeter spatial resolution using portable and low-profile imaging apertures, 3) and enable long-distance (>20m) imaging in adverse conditions. Additionally, the synergy between THz NLoS and communication systems will be explored to enable novel localization and channel estimation techniques.

The THz spectrum (300GHz to 10THz) is an active research area for imaging systems and wireless communications. At terahertz frequencies, most building surfaces are rough, thus making the diffuse scattering a possibility. Nevertheless, the specularly reflected component is dominant and can be used to enable imaging of the hidden objects [28].

1.6 Prior Work on NLoS Imaging Methods

Work on NLoS can be traced as far as the 1960s when Goodman et al. [29] proposed a holography technique to reconstruct obscured wavefront from the object after hitting a diffusive surface. Small changes in the refractive index of the medium can diffuse light. Hence the phase of the wavefronts is distorted, and the image is degraded by atmospheric factors. Goodman proposed a technique of using a reference beam along with the object beam, and even though individually both the beams are disturbed, they are affected in the same way by the diffusive object. This effect makes the relative phase shift between the beams tenable. Later in 1968, Kogelnik et al. [30] used the same theory but added a lens focusing system to enable remote sensing. Even though both techniques focus on imaging an object obscured by the light passing through the diffusive surface, the same theory is used for reconstruction in NLoS technology. In around the corner, wavefronts distortion is caused by scattering of the light on the diffusive surface, which is used for reflection instead of transmission through the medium. This technique has a limited field of view because of the lens system and is not robust enough to fit the practical scenarios. Lens system with a narrow field of view adds speckle to the image.

There is also another technique in holography which used SLM (spatial light modulators) and memory effect of the optical waves to reconstruct the NLoS scenario. SLM is used to

control the wavefront pattern that is a phase at each point in space. Hence we can obtain any pattern of wavefronts even the inverse pattern of obscuration caused by the diffusive surface. Feedback systems are used to adjust the random phase of SLM [19]-[21] until the proper image is obtained. This technique has a limited field of view because of the specific pattern of SLM should be changed every time we change the focus point on the diffusive surface. The memory effect defines that in a small area around the current focal point of the beam still the same SLM pattern can be used to reconstruct or correct the obscured images.

Time of flight imaging [1]-[2], is also made possible in optics in real-time by femtosecond pulsed laser and camera. This optical equipment can sample the light signal in the order of picoseconds. Light transport matrix and triangulation are used to locate the pixel in the geometry. The light transport matrix has information on the interaction of different reflections in the object scene. The patch on the body of the object has the locus of the ellipse, which is corrected using advanced optimization algorithms. The techniques above have a limited field of view, and they are light-based, so they suffer from the heavy diffusive property of the light waves.

Some microwave RADAR techniques are also tested for NLoS application. Different localization algorithms are used in each one and have the assumption of data on the background scene is available [25]-[27]. Localization algorithms are necessary to correct the position of the objects in the reconstructed image. The microwaves have longer wavelengths, which make the resolution limited, and materials are transparent, which makes the image even more cluttered. Optical systems are diffused Omni directionally

unless the surface is extremely smooth, this makes the practically questionable because of the signal to noise reconstruct obscured wavefront from the object after hitting a diffusive surface. Little changes in the refractive index of the medium can diffuse the light; hence, the phase of the wavefronts is obscured, and hence, the resolution of imaging is limited by atmospheric factors.

1.7 Outline:

With the detailed description available in the above sections, the logical choice for the implementation of NLoS technology is using the Terahertz spectrum. Chapter 2 describes the backpropagation imaging algorithm in two different points of view. EM view gives us an understanding of the physics underlying the imaging algorithm, but we need a signal processing point of view to understand the implementation of the back-propagation algorithm. We will present the derivation for a planar scanning synthetic aperture with monostatic, bistatic wide band geometry and also present the SAR aperture sampling requirements. In imaging, the spatial frequency domain (k-space) is used to analyze the imaging capability of the system. Chap.3 presents the results of a simulation using the above algorithm for LOS images. In chap.4 first, we talk about our novel idea for NLoS imaging and present the results. The final chapter discusses future work that can be done to improve this technique and also put forward some conclusions.

2 BACK PROPAGATION ALGORITHM FOR IMAGE RECONSTRUCTION

Imaging is defined as the measurement of the target reflectivity function from the scattered data collected over the synthetic aperture [7],[31]. Imaging algorithms accomplish this task by focusing the scattered signal within range and cross-range domain. The range corresponds to the depth of the target while the cross-range corresponds to the azimuthal dimension. Focusing or compression in both domains can be achieved with different algorithms derived from valid approximations. In this chapter, we will start with basic electromagnetic equations relating to the incident field, scattered field, and object reflectivity function. Scattered fields are perceived from a signal processing perspective, and algorithms are deduced to form an image from the data collected over a planar aperture. Soumekh [31] has implemented the idea of holography using SAR techniques to derive the back-ward wave propagation algorithms. The algorithm for SAR used in Soumekh can be extended to fit the multi-static case. The 3D backpropagation algorithm for a multi-static antenna scenario is formulated in both space and spatial frequency domain. Fourier transforms used in several steps to move between domains, and hence we investigate their effect in setting the sampling and resolution limits. Techniques such as matched filtering and interpolation, which are intermediate steps in the back-propagation algorithm, are also studied. Each step of the backpropagation algorithm is explained, and an example of a 2D target scenario is presented.

2.1 Deriving the Scattering Equation using Born Approximation

Like all other electromagnetic problems, the scattering phenomena are solved using the Helmholtz equation. The wave equation for the incident wave is homogenous, but the wave equation for the scattered field results in an inhomogenous Helmholtz equation (2.1), which depends on the total field. Proof for these equations is mentioned in the literature [10],[31]-[33].

Here $E = E^s + E^i$ is the total field, E^i is the incident filed and $E^s$is the scattered field.

$$\nabla^2 E^s + k_0^2 E^s = -o(r).E \tag{2.1}$$

where k_0 is the free space wavenumber represented and c_0 represents the speed of light in vacuum.

$$k_0 = \frac{\omega}{c_0} \tag{2.2}$$

$o(r)$ In (2.3) is the object function, and it describes the variation of the permittivity or reflectivity through the body of the scattering material. Object function gives the reflectivity of an object in relation to co-ordinates. Hence, it has information about the geometry of the scattering body. All the imaging algorithms will be used to extract the object function out of the linear scattering equation.

$$o(r) = k_0^2(\varepsilon_r^c(r) - 1) \tag{2.3}$$

$\varepsilon_r^c(r)$ is the relative permittivity of a material, r is the radial distance.

The non-homogenous differential equation shown in (2.1) is solved using spherical greens function, which represents the outward propagating spherical waves from the source. Using Greens theorem [10] the (2.1) can be represented in the volume integral as

$$E^s(r) = \iiint_v o(r').E(r').G(r-r')dr' \tag{2.4}$$

where

$$G(r) = \frac{e^{-jk_0 r}}{4\pi r}$$

The equation shown above is a non-linear equation because of the total field inside the integral. Solving a nonlinear equation of large imaging geometries is computationally impossible. The Born approximation is used to convert the non-linear scattering equation to a linear one by considering the weak scattering assumption. For a weak scattering object, the scattered field can be neglected when compared to the incident field. Hence the total field can be represented as

$$E \approx E^i$$

Now using the Born approximation, the linearized scattering equation is given by

$$E^s(r) = \iiint_v o(r').E^i(r').G(r-r')dr' \tag{2.5}$$

$$E^s(r) = o(r).E^i(r) * G(r) \tag{2.6}$$

The superposition above represents a linearized physical scattering phenomenon. Incident field effected by the object function in (2.6) is propagated through the space using spherical wave-fronts. All the scattered wavefronts are superposed or integrated to form the scattered field (linear problem).

2.2 Scattering Equation for Imaging Geometry

In the previous section, the object function is inside the convolution integral of the scattering equation, and hence, retrieving the reflectivity of the target requires inversion [10]. Linearized Helmholtz scattering equation using Born approximation is the basis for the reconstruction algorithm. The earliest imaging algorithms like RDA (Range-Doppler Algorithm) and polar format algorithm, which is a polar representation of RDA, used the approximation of plane waves to retrieve the reflectivity of the target [31]. This approximation considers a planar wavefront and thus adds an error when the imaging is performed in a near field target because it does not account for the wavefront curvature. Spherical wave approximation for the incident and scattered fields instead of the planar eliminates this approximation. Though this step adds considerable pressure on computation efficiency, the resolution of the target cannot be spared. Now the problem of the wavefront curvature is handled using the Fourier transform, which plays a vital role in all of the spatial frequency-based algorithms like RMA (range migration algorithm) and PMA (phase shift migration algorithm) [33]. Physical interpretation behind using the Fourier transform is to break the spherical wavefront into a combination of plane waves, as shown in Figure 2-1,

and process the data using phase compensation. Thus, the only limitation to the image resolution is set by the wavelength of the incident wave, geometry of the aperture, and the distance between the planar aperture and the target.

An imaging algorithm at this point can be understood as the correlation of the scattered fields with the incident fields to derive the object function. The target is illuminated with plane waves from different view angles to correlate the position accurately.

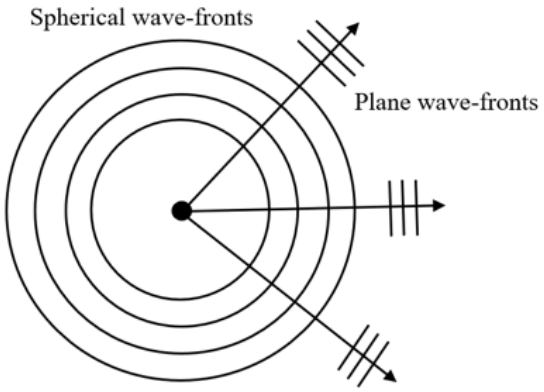

Figure 2-1 Spherical wavefronts can be expressed as a superposition of planes waves

is for a general multi-static case in which transmitter and receiver positions are different and these. In the multi-static imaging method, one transmitter illuminates the target, and the scattered field is received over all the receivers, which are then followed by the next transmitter transmitting the incident wave. This procedure is repeated through all the transmitters over the whole bandwidth.

Planar geometries can be easily analyzed using the rectilinear or Cartesian coordinate system. Planar geometry is considered for transmitter and receiver with a multi-static configuration as shown below in Fig 2.2 with target space to be at a minimum range of Z_0.

The transmitter and receiver are located using the coordinates (x_t, y_t, z_a) and (x_r, y_r, z_a) respectively on the plane of a transceiver. The algorithm assumes point targets to be defined by O(x, y, z), and each volume unit block in the 3-D image is called a voxel, similar to a pixel in a 2-D image.

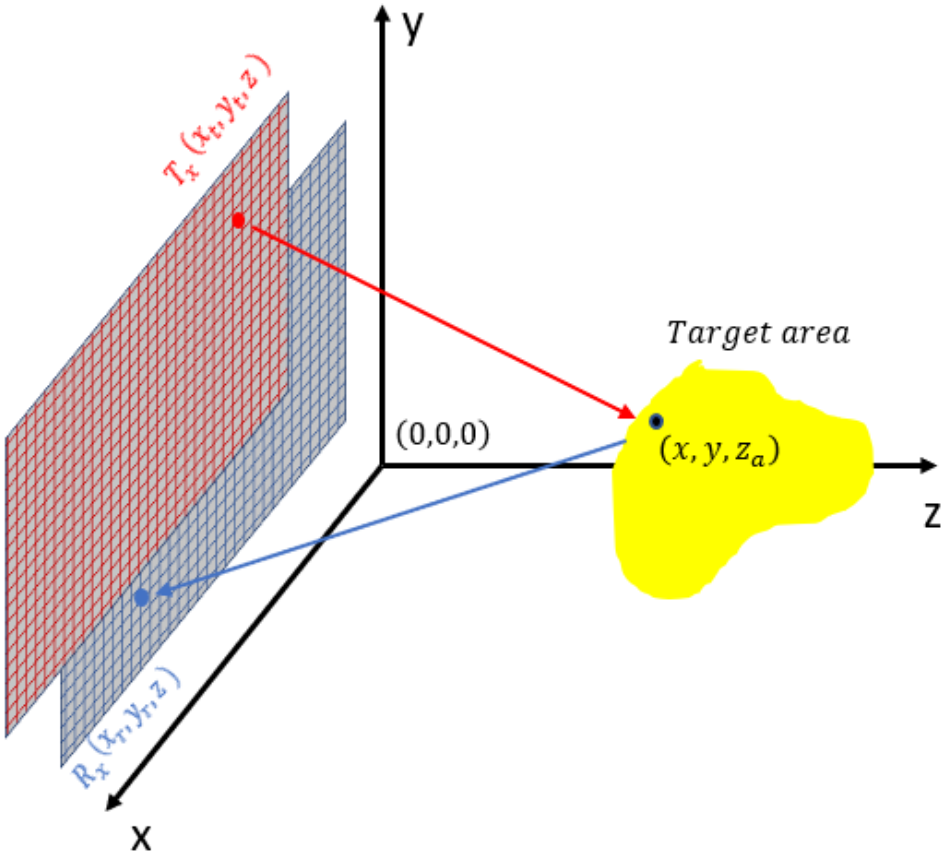

Figure 2-2 Rectangular imaging co-ordinate system with the generic multi-static configuration

Now the variables in eq. 2.6 are replaced using the associated geometry in Figure 2-2.

$$O(r') = O(x, y, z) \tag{2.7}$$

$$E^s(r) = s(x_t, x_r, y_t, y_r, k) \tag{2.8}$$

$$E^i(r') = exp\left(-jk\sqrt{(x_t - x)^2 + (y_t - y)^2 + (z_a - z)^2}\right) \tag{2.9}$$

$$G(r - r') = exp\left(-jk\sqrt{(x_r - x)^2 + (y_r - y)^2 + (z_a - z)^2}\right) \tag{2.10}$$

Here spherical greens function is used in compliance with the near-field assumption, and the source is assumed to be isotropic. The terms related to the amplitude are dropped from the derivation because of the slowly varying nature of these terms when compared to phase variation over the aperture. If we substitute the terms 2.7-2.10 in the 2.6, we can deduce the mathematical model for the scattered field recorded at on the receiver located at (x_r, y_r) when the transmitter located at (x_t, y_t) is radiating a signal of frequency k.

$$s(x_t, x_r, y_t, y_r, k) = \int_x \int_y \int_z O(x, y, z) \tag{2.11}$$

$$exp\left(-jk\sqrt{(x_t - x)^2 + (y_t - y)^2 + (z_a - z)^2}\right).$$

Tx term

$$exp\left(-jk\sqrt{(x_r - x)^2 + (y_r - y)^2 + (z_a - z)^2}\right). \qquad \boxed{\text{Rx term}}$$

$$dx\ dy\ dz\ .$$

2.3 Imaging Algorithm

The total scattered field in (2.11) depends on phase delays from the transmitter to the target and from target to the receiver. This phase compensation of the phase fronts can be done by a signal processing technique known as matched filtering. Matched filtering can be applied to (2.11) in space and spatial frequency domain [10]. The spatial frequency technique is known as a range shift migration [33].

2.3.1 Spatial Domain Algorithm:

The spatial domain technique uses the direct correlation at each voxel of the image concerning transmitter and receiver positions. Matched filtering technique in the space domain is shown below in (2.12) for continuous targets. However, the computer algorithms deal with the discrete data and hence (2.12) is modified to (2.13).

$$\hat{O}(x, y, z) = \int_k \int_{y_r} \int_{x_r} \int_{y_t} \int_{x_t} s(x_t, x_r, y_t, y_r, k) \qquad (2.12)$$

$$\left(exp\left(-jk\sqrt{(x_t - x)^2 + (y_t - y)^2 + (z_a - z)^2}\right)\right)^*.$$

$$\left(exp\left(-jk\sqrt{(x_r - x)^2 + (y_r - y)^2 + (z_a - z)^2}\right)\right)^*\ dx\ dy\ dz$$

$$\hat{O}(x,y,z) = \sum_{k}\sum_{y_r}\sum_{x_r}\sum_{y_t}\sum_{x_t} s(x_t, x_r, y_t, y_r, k). \tag{2.13}$$

$$\left(exp\left(-jk\sqrt{(x_t - x)^2 + (y_t - y)^2 + (z_a - z)^2}\right)\right)^*$$

$$\left(exp\left(-jk\sqrt{(x_r - x)^2 + (y_r - y)^2 + (z_a - z)^2}\right)\right)^* \, dx\, dy\, dz$$

Here, the correlation eliminates the signals from other voxels because they add destructively with conjugate terms in the (2.13), whereas the terms from the voxel in question add constructively. Hence this voxel leaves a blip in the image. The size of the blip is usually essential to quantify the quality of the image called resolution. Now the function is repeated for each target position. The algorithm for the spatial domain is given below in Figure 2-3.

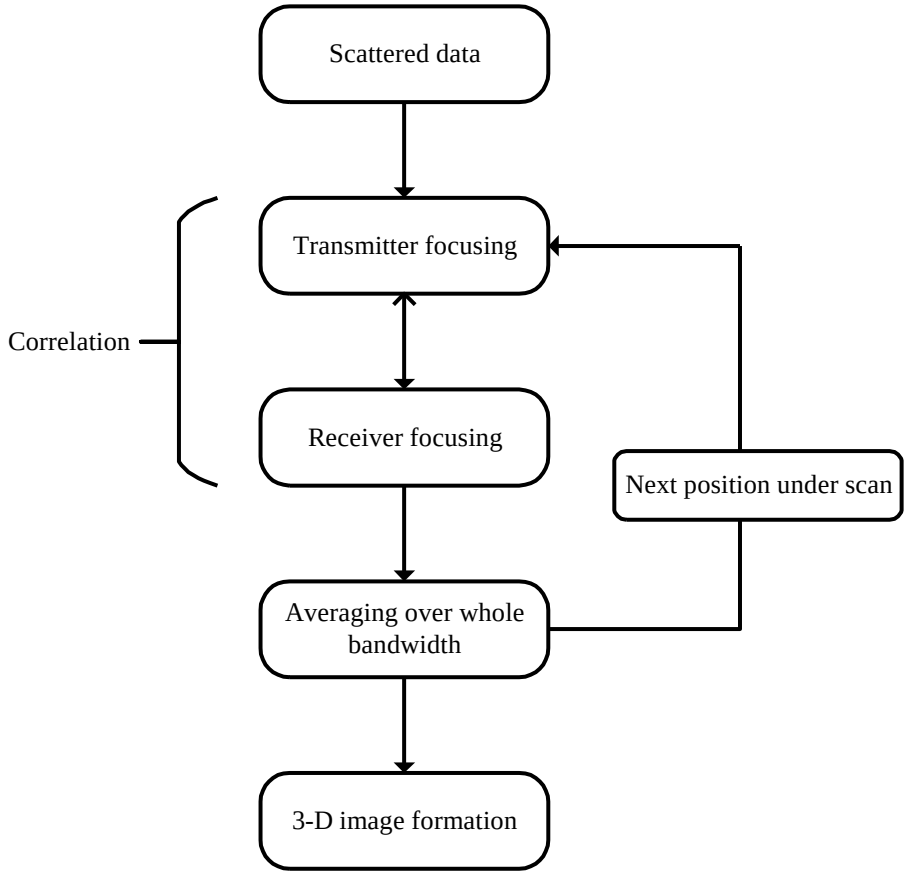

Figure 2-3 Flow diagram for spatial domain back-propagation algorithm

2.3.2 Spatial Frequency Domain Algorithm:

The spatial algorithm, though easy to implement and more accurate, has more computational requirements. Hence this limits the usage of the algorithm for higher arrays and target areas. The spatial frequency domain algorithm compared to the space domain adds small error due to interpolation problems but is computationally more efficient. Hence the spatial frequency algorithm is likely the choice for all practical applications where there is a limitation on the processing power of the system to obtain a real-time image [10].

Phase compensation is not possible in a spatial domain because of the non-linear phase function shown in (2.13). Wavefront curvature is compensated in the frequency domain by breaking down a spherical wave to the linearized sum of plane waves. When each of these plane waves is modulated by the object function in the total volume occupied gives the Fourier domain of the object, as shown in (2.14). The phase shift migration technique is chosen because of its optimized treatment between the resolution and computational efficiency. The general multi-static reflected signal is a five-dimensional signal containing coordinates of the transmitter, receiver, and the frequency as in (2.14). Four-dimensional Fourier transform is applied because of four cross-range coordinates, two concerning the transmitter and the other two concerning the receiver.

$$S(K_{xt}, K_{yt}, K_{xr}, K_{yr}, k) = \int_x \int_y \int_z O(x, y, z).F_{4D}[Tx\ term.Rx\ term]\, dx\, dy\, dz \quad (2.14)$$

Asymptotic methods like MSP (method of stationary phase) are to be employed for solving the Fourier integral of the spherical phase functions. According to MSP, the significant part of the integral comes from the terms which have a stationary phase throughout the aperture. Oscillatory components add destructively and will result in a minute sum and hence, neglected by this approximation. Hence the MSP holds good for the target point and leaves out all the other terms in the integral expansion.

Here we will concentrate on the approximations where MSP is valid. MSP is derived using the approximation made below.

$$k > 0 \tag{2.15}$$

$$z > z_a \tag{2.16}$$

$$(k^2 > (k_{xt}^2 + k_{yt}^2)) \; \forall \; (z > z_a) \tag{2.17}$$

Lower wavelength propagating modes with a distant target from the scanning aperture will hold good for the MSP. Lower wavelength corresponds to the higher k values. Only propagating modes are taken into account, which even is the case for the algorithm. In our case, the imaging is performed in terahertz bands, which have significantly high values of k.

Fourier transform of the phase terms using MSP is derived from being

$$F_{4D}[Tx\ term.Rx\ term] = F_{2D}[Tx\ term].F_{2D}[Tx\ term] \tag{2.18}$$

$$F_{2D}[Tx\ term] = exp\left(-j\sqrt{k^2 - k_{xt}^2 - k_{yt}^2}(z - z_a) - jk_{xt}x - jk_{yt}y\right) \tag{2.19}$$

$$F_{2D}[Rx\ term] = exp\left(-j\sqrt{k^2 - k_{xr}^2 - k_{yr}^2}(z - z_a) - jk_{xr}x - jk_{yr}y\right) \tag{2.20}$$

Substituting (2.18)-(2.20) in (2.14) we derive

$$S\left(K_{xt}, K_{yt}, K_{xr}, K_{yr}, k\right) = exp\left(j\sqrt{k^2 - k_{xt}^2 - k_{yt}^2}z_a + j\sqrt{k^2 - k_{xr}^2 - k_{yr}^2}z_a\right). \tag{2.21}$$

$$\int_x \int_y \int_z O(x, y, z).exp(-jk_x x).exp\left(-jk_y y\right).exp(-jk_z z)\ dx\ dy\ dz$$

Where

$$k_x = k_{xt} + k_{xr} \tag{2.22}$$

$$k_y = k_{yt} + k_{yr} \tag{2.23}$$

$$k_z = \sqrt{k^2 - k_{xt}^2 - k_{yt}^2} + \sqrt{k^2 - k_{xr}^2 - k_{yr}^2} \tag{2.24}$$

2D Fourier transform of the object function is

$$O\left(k_x, k_y, z\right) = \int_x \int_y O(x, y, z)\ exp(-jk_x x).exp\left(-jk_y y\right)\ dx\ dy \tag{2.25}$$

Now the term inside the integral of (2.25) looks like a Fourier transform of the object function. Replacing the Fourier transform of the object function gives,

$$S(K_x, K_y, k) = exp\left(j\left(\sqrt{k^2 - k_{xt}^2 - k_{yt}^2} + \sqrt{k^2 - k_{xr}^2 - k_{yr}^2}\right) z_a\right). \int_z O(k_x, k_y, z).exp(-jk_z z)\, dz \quad (2.26)$$

The equations to derive the expression for the estimated object function by the theory of matched filtering is

$$O(K_x, K_y, k) = exp\left(j\left(\sqrt{k^2 - k_{xt}^2 - k_{yt}^2} + \sqrt{k^2 - k_{xr}^2 - k_{yr}^2}\right) z_a\right). \int_k S(k_x, k_y, z).exp(-jk_z z)\, dk \quad (2.27)$$

If the reference plane of a transceiver is origin ($z_a = 0$), then

$$O(K_x, K_y, k) = \int_k S(k_x, k_y, z).exp(-jk_z z)\, dk \quad (2.28)$$

$$\hat{o}(x, y, z) = \int_{k_x} \int_{k_y} O(k_x, k_y, k)\, exp(jk_x x).exp(jk_y y)\, dkx\, dky \quad (2.29)$$

Fourier theory applies to the signals which are uniformly sampled, but the case in (2.29) does not comply. Even though kx and ky are moving uniformly, the nonlinear expression for kz makes it non-uniformly sampled. This nonuniformity in the sampled signal will lead to the defocusing error if the inverse Fourier transform is used directly. So, the signal should be mapped to a uniformly spaced rectangular grid. A high-frequency small aperture

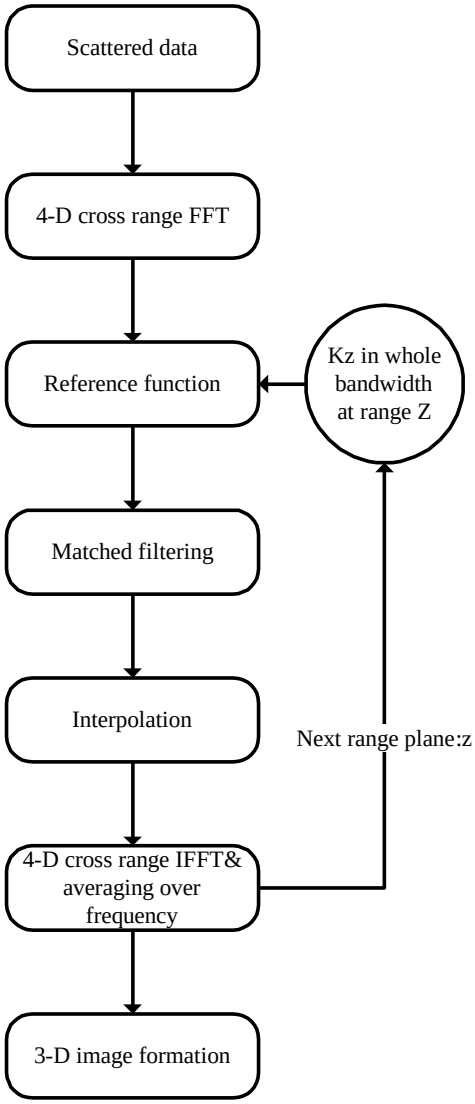

Figure 2-4 Flow diagram for spatial frequency domain backpropagation algorithm

scanning systems k is significantly large compared to the cross-range spatial frequency terms kx, ky, and hence the interpolation step will not affect the resolution as in the case of lower frequency imaging systems.

The (2.29) is practically implemented, as shown in Figure 2-4. The first step is to acquire the data over the whole receive aperture in the total bandwidth and store them digitally. Next, the Fourier transform is applied in all the cross-range domain for the received data. Now the phase of the spatial frequency data is compensated using the matched filtering technique. Reference function is chosen according to the range plane we need to image. Hence the algorithm gives out images of the plane after plane, as shown in Figure 2-5. Interpolation should be performed if necessary to avoid defocusing of the target. The final step is to transform back the data to the space domain.

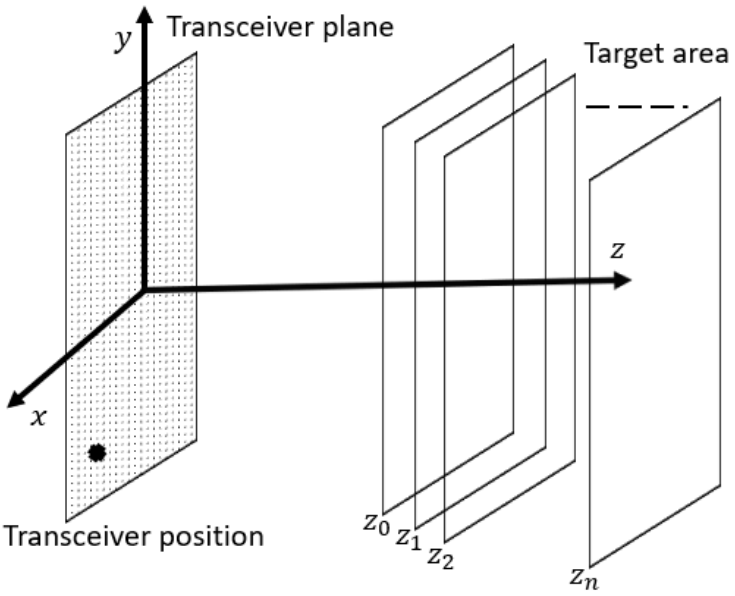

Figure 2-5 Back-propagation algorithm focuses the image of a plane at a distance Z_0, Z_1 , Z_2 up to $Z_n$succeesively.

2.4 Resolution and Sampling Properties

Sampling and resolution are essential terms in quantifying the imaging method and geometry. Using Fourier transform in the imaging algorithm also necessitates the study of sampling and resolution parameters to avoid aliasing errors. Sampling gives the maximum distance between two elements in the transceiver geometry while the resolution outlines the minimum distance that two objects need to be placed in order to tell them apart successfully. As in the time-frequency domain, spatial- spatial frequency domain occupancy sets the resolution limits. In imaging, the spatial frequency occupancy of geometry is known as the *k*-space. Typically, the diffraction of an EM wave restricts the spatial resolution to less than $\lambda_{min}/_2$, where λ_{min} is the minimum wavelength of the maximum frequency of the transmitted signal.

Some literature shows the derivation of spatial frequency limits using co-ordinate transformation while others derive it directly from the phase function; nonetheless, we arrive at the same constraints. The phase of the spherical wave received is

$$\begin{aligned}\phi(x_t, y_t, x_r, y_r, k) \\ &= 2.k\left(\left(\sqrt{(x-x_t)^2+(y-y_t)^2+(z-z_a)^2}\right)\right. \\ &\left.+\left(\sqrt{(x-x_r)^2+(y-y_r)^2+(z-z_r)^2}\right)\right)\end{aligned} \tag{2.30}$$

From simple derivative theory, we know that the rate of change of phase is the frequency, and hence the derivative of the above (2.30)concerning the respective cross-range gives us the instantaneous frequency component in the signal. Finding the minimum and maximum limits of this derivative gives the range of k-space or the k-space support in the respective

cross-range domain. From the Fourier theory, the resolution limits in 3-D can be defined as

$$\delta_x = \frac{2\pi}{\Delta k_x} \tag{2.31}$$

$$\delta_y = \frac{2\pi}{\Delta k_y} \tag{2.32}$$

$$\delta_z = \frac{2\pi}{\Delta k_z} \tag{2.33}$$

$\Delta k_x, \Delta k_y \; and \; \Delta k_z$ are derived using the method described above in [10],[31],[33]. The resolution depends on the position of the point target concerning SAR. Target centered on SAR in cross-range has a better resolution because of the highest occupancy of the k space. Hence the target point far away from the center of the SAR has a very low k-space range and hence the worse resolution. The range and cross-range resolution formulae are given below are for the target positioned at the center of cross-range aperture.

$$\delta_x = \delta_y = \frac{c}{4f^{max}} \sqrt{4\left(\frac{L}{D}\right)^2 + 1} \tag{2.34}$$

Where

$L = Z - Z_a$ is the distance between the target and the aperture plane

D is the length of the aperture

f^{max}, f^{min} are the maximum and minimum scanning frequencies

Δf is the bandwidth of the signal

$$\delta_z = \frac{c/2}{\Delta f + f^{min}\left(1 - \frac{1}{\sqrt{1 + \frac{1}{2}(D/L)^2}}\right)} \tag{2.35}$$

The nonlinear spherical phase function of the return signal, as shown (2.3), needs to be uniformly sampled before the application of the Fourier transform. Nyquist sampling theorem is used to find the sampling limits for the antenna aperture. The instantaneous phase of the signal can be found using the derivative concerning the corresponding cross-range coordinate. The maximum and minimum of this function give the total k-space occupied by a target.

Here we can notice that based on the target coordinates, the k-space occupied varies, and hence, the resolution of the point varies. Physically the point targets closer to the center of the cross-range have better resolution than the target at the end of the aperture.

3 LINE OF SIGHT IMAGING SIMULATION AND RECONSTRUCTION

3.1 Ideal Target Simulation and Reconstruction

As mentioned in the previous section, the general multi-static algorithm is applicable for any configuration of transmitter and receiver array. In this section, we will convert the multi-static algorithm to a simple monostatic case and apply it to form the image of an analytic target. As this example is presented for clarification, no further complexities like frequency-dependent reflection are assumed regarding the object geometry. We will present the signal operation in each step of the algorithm, as mentioned above. We choose one range and cross-range domain, so scattered data must be collected over the one cross-range and in a band of frequencies.

In monostatic geometry, both transmitter and receiver lie in the same position and hence

$$x_t = x_r$$

Moreover, as we are considering only one cross range, the dependency on y terms is dropped. The interpolation term is

$$k_z = 2 * \sqrt{k^2 - k_x^2}$$

For the reconstruction, we need to apply one dimensional Fourier transform for the raw data along the cross-range x dimension to convert it to a spatial frequency domain.

$$O(K_x, K_y, k) =$$

$$\int_{k} S(k_x, z).exp(-jk_z z)\, dk$$

$$\hat{o}(x,z) = \int_{k_x} O\left(K_x, K_y, k\right).exp(jk_x x)\ \ dkx$$

Bandwidth, frequencies, and sample spacing are selected according to the resolution requirements. In this section, we will demonstrate the imaging algorithm with a simple 2-D (range, cross-range) monostatic example. The scattered signal is formed from a point target, which is 60cm away from the SAR and an aperture size of 28cm, as shown in Figure 3-1. The bandwidth of 220-330GHz is selected with a 55MHz spacing for the Terahertz measurements. The above system specification will give us the image of a target with proper resolution though hard to accurately derive. When there are several targets placed at different positions, then the worst-case or the lowest sampling distance is selected. Figure 3-2 shows us the real part of the received data at a 275GHz frequency over the whole aperture.

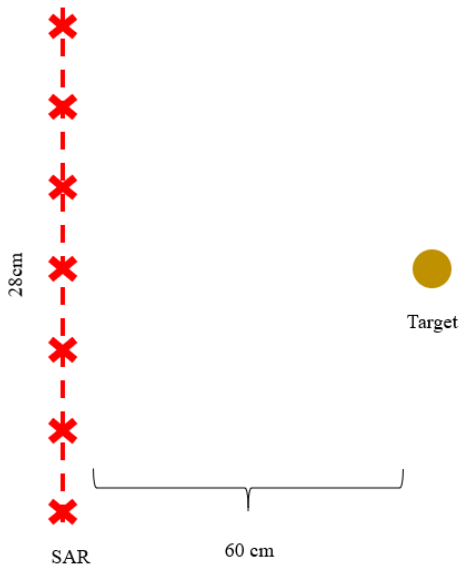

Figure 3-1 SAR 1-D monostatic simulation geometry with a sphere as the target. Crosses represent the scanning points on the aperture

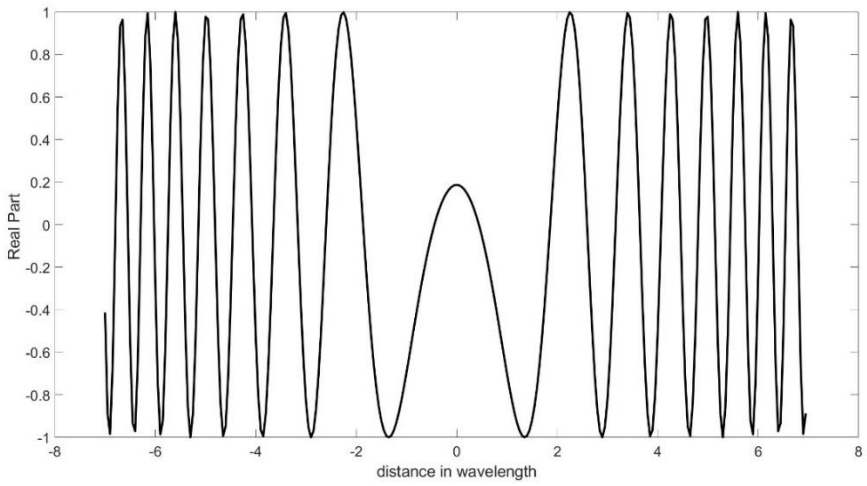

Figure 3-2 Real-part of the received signal over the mono-static scanning aperture shown in above Figure 3-1 with X-axis representing the distance from the center of the scanning aperture

Now the image is formed with a point target placed at 60 cm range, as shown in Figure 3-3, and then multiple targets are placed at different positions to observe the resolution change. As a rule of thumb, the closer the target to the center of SAR better the resolution.

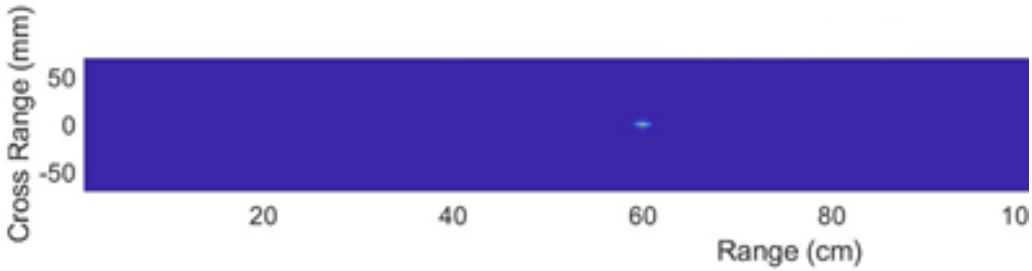

Figure 3-3 Imaging a target placed 60cm away from the scanning aperture, light blip represents the position of the target.

In Figure 3-3, the horizontal axis represents the range, and the vertical axis represents the cross-range, and hence, we can imagine the SAR is present across the cross-range at the 0cm range. We can see a sinc shaped blip at the 60cm range at the center of the cross-range, which corresponds to the target.

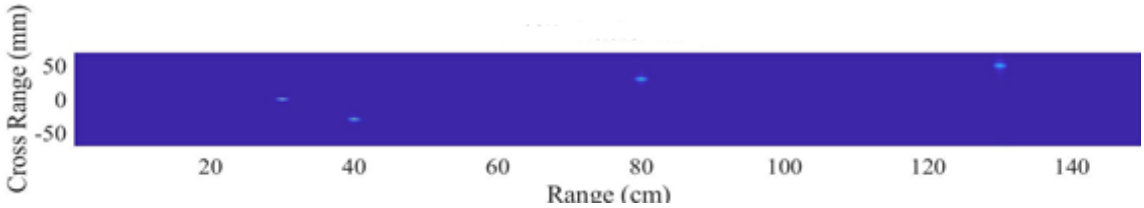

Figure 3-4 Imaging multiple targets at 30cm, 40cm, 80cm, and 130cm

We can observe four targets in the reconstructed image placed at different positions in Figure 3-4. Targets are named according to their range as target-1 at 30cm, target-2 at 40cm, target-3 at 80cm and target-4 at 130cm. Target-1 is at a range of 30cm away from the SAR, and at the center of the cross-range and hence the closest of all, thus we can see the smallest blip on the surface plot compared to all other targets.

3.2 EM Simulation and Reconstruction:

Analytic target reconstruction is the proof for the backpropagation algorithm in an ideal isotropic source and target environment, but this section alone is not enough for the practical applicability of the backpropagation. The distributed target structures and non-isotropic nature of practical sources add additional complexity to focus on an image. As with all the electromagnetic applications, a 3D EM simulation is necessary for the practical appreciation of the chosen imaging method. FEKO is chosen for the fast and straightforward simulation environment, which uses Integral Equation MOM [35]. The multi-static 3D algorithm in the (2.29) is modified to fit the corresponding 1D or 2D cross-range monostatic cases. The modified algorithm is applied to the simulated data to reconstruct the image of the target using MATLAB[36]. 2D (range and cross-range) algorithm is enough to prove the 3D method because it contains both the range and cross-range property along 1D, and hence the algorithm is derived for this case. 2D(range and cross-range) is not simulated using FEKO because of the computational burden due to high bandwidth scanning for a specific range. A pyramidal horn antenna with a 20dB gain is

used to sweep across the SAR to verify the applicability of the horn antenna for imaging. PEC(perfect electric conducting) sphere with a radius of λ is chosen as the target for good SNR(signal to noise ratio) and resolution properties

3.2.1 1D Monostatic Simulation Example

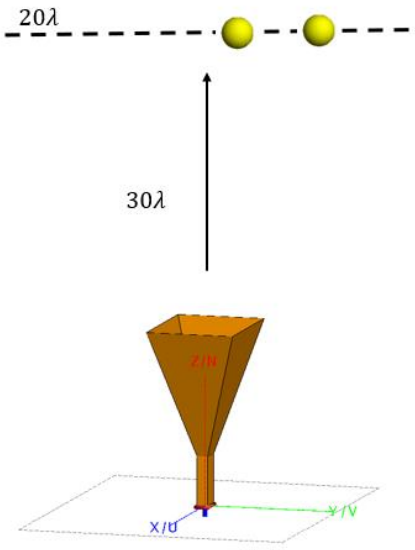

Figure 3-5 1-D mono-static imaging setup using 20dB gain pyramidal horn antenna, sphere represents the target which is placed at a distance of 35λ from the phase center of the antenna

The simulations are done at 20GHz with a 20dB gain pyramidal horn antenna. The simulated geometry using FEKO is given in above Figure 3-5. The horn antenna is swept across a length of 20λ and is placed at a distance of 35λ away from the target aperture. The range of the target is considered from the phase center of the horn antenna. The target is positioned 3λ away from the center of the aperture in the cross-range. The reconstructed image is given in Figure 3-6; Here, we can observe a little distortion added due to the curved surface scattering happening at the target(sphere).

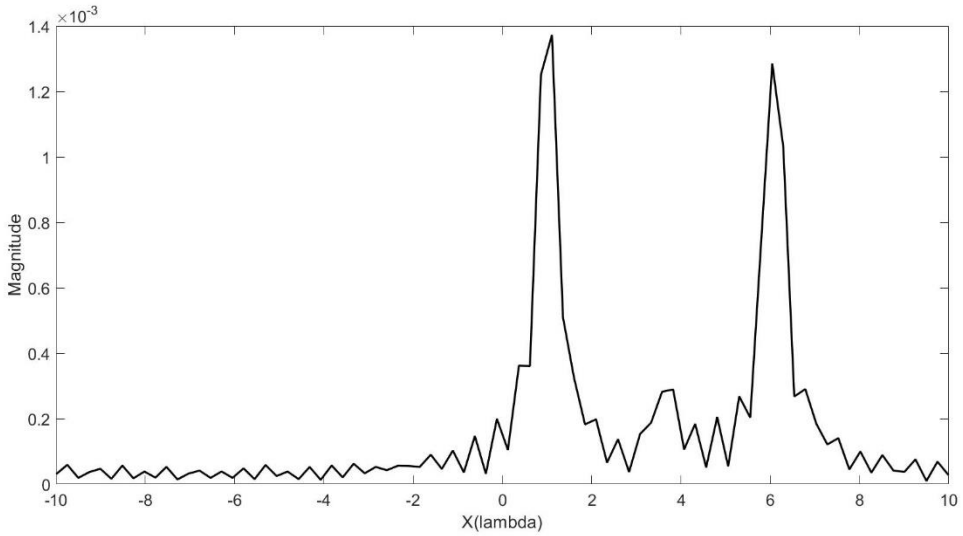

Figure 3-6 Reconstructed image of two targets of the setup shown in the above Figure 3-5.

3.2.2 2D-Cross Range Monostatic Imaging Example

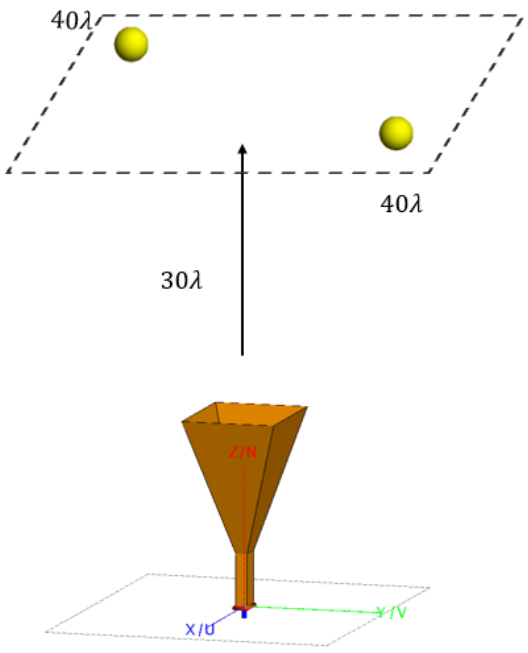

Figure 3-7 2-D mono-static imaging setup using 20dB gain pyramidal horn antenna, Target sphere's are located at a distance of 14λ from the phase center of the antenna

The simulations are being carried out at 20GHz with a 20dB gain pyramidal horn antenna. The simulated geometry using FEKO is given below in Figure 3-7. The horn antenna is swept across a length of 10λ in both the cross-range domain's X and Y. The range of the target is considered from the phase center of the horn antenna to the target plane, which is at a distance of 15λ away from the origin. Two spherical targets with the radius of λ are spaced approximately at 14λ from their centre. Final reconstructed image was shown in Figure 3-8.

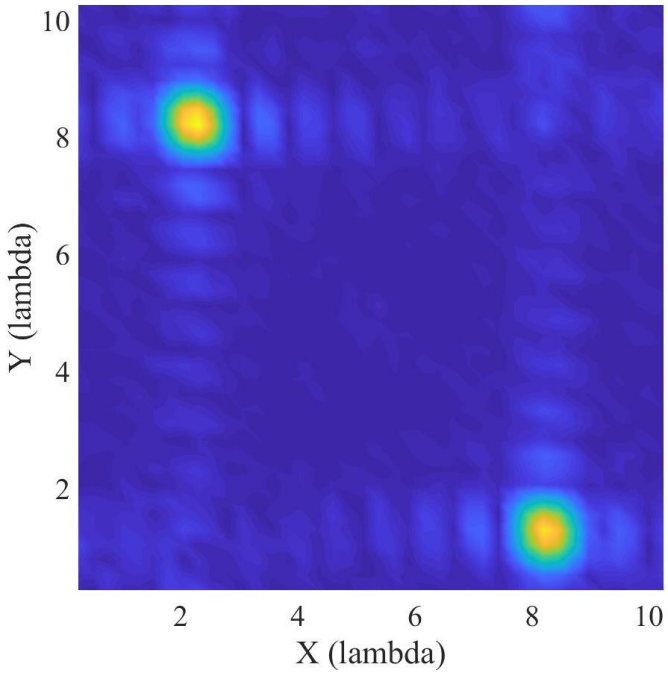

Figure 3-8 Final reconstructed image exposing two spherical targets placed along the two cross-range domain X and Y.

4 NLOS IMAGING MEASUREMENTS AND RESULTS

This chapter presents a detailed description of the measurement set-up and process for NLoS imaging. 3-D imaging requires the scattered signal to be collected across the aperture at different positions and across the total bandwidth. High-resolution pictures need a high scanning area and more bandwidth. SAR with terahertz spectrum provides a solution for high resolution with ease of measurement set-up procedure. In the first section, the SAR set-up and the scanning process is discussed. In the latter section, data collection, storage, and reconstruction are discussed.

This process of data collection, storage, and image reconstruction is called the quasi-real-time reconstruction. Physical aperture scanning can make this process quick and efficient, but the construction of effective radiating sources at terahertz adds a constraint. Here the targets are static, and hence no doppler shift is expected at the receiving aperture. In the later section, examples for both lines of sight images and non-line sight images are presented. For the same scanning aperture, resolution degrades with range away from the aperture. The advantages of terahertz sensing for NLoS technology are evident from these images of the non-line of sight scenario.

Initial reconstruction of the non-line of sight scenario will place the targets in a wrong position as the orientation of the target is not available to the SAR. Hence, the non-line of imaging requires employing some localization techniques. Mirroring, based on the orientation of the wall, is employed to place the object in the correct positions. There are two different set-ups for non-line of sight imaging, one with a single wall and the other with two walls with targets in front of both of them. The latter set-up adds complexity to

the reconstruction procedure. The two-wall scenario also presents the complexity of the practical environment as the walls are curved and oriented arbitrarily.

4.1 SAR Reconstruction Procedure

Isotropic source gives the best resolution, but there are no practical non-directional sources designed for terahertz frequencies. Diagonal horn antenna, even though it has high directivity and low beam-width as opposed to an isotropic source, has a high bandwidth and polarization purity. Diagonal horn antenna in the range (220-330) GHz gives better range resolution with higher radiated power for good SNR in the received signal. Scattering and data collection are done using VNA with frequency extenders [37]. Frequency extenders give the capability to a network analyzer to work beyond its operating frequency range using RF multipliers.

The translation stage is used to simulate synthetic aperture. Scattered data from the target is collected over a 13cm of an aperture with 1mm of sampling distance. The translation stage carries the horn antenna along with the frequency extenders, which are, in turn, connected to a VNA through flexible, low-noise coaxial cables. VNA and translational stages are connected to a computer through a router that sends the control signal and stores the return data. The control code is written using Lab-view because the control blocks for VNA (Rhode and Schwarz) and Translational stages (Thor labs) are available from the respective manufacturers. All the settings for the VNA like the bandwidth, number of frequency points, IF (Intermediate frequency) bandwidth, and calibration file are passed

through the computer. Hence at each scanning point, the terahertz signal is generated, scattered, collected, and stored on the computer.

4.2 Line of Sight Imaging Setup

We are considering a mono-static scenario as opposed to a generic multi-static configuration given in Chapter 2. A general multi-static wideband imaging scenario has the transmitters and receivers looking from directions that need to be modified by placing the same co-ordinates for the transmitting and receiving aperture. We need to apply 2-D Fourier transform on the raw data to transform it into the plane wave domain and apply the focusing function to obtain the image at a particular range. The final stage of reconstruction can be done by averaging over the whole bandwidth or a 1D inverse Fourier transform.

The target is chosen to be a stationary metallic long screw which has a cylindrical aperture and a good RCS (RADAR Cross-Section) at all angles. Reconstruction is very much similar to the simulation presented in Chapter 3. Practical imaging result for a LoS image is given in Figure 4-1.We can observe a blip at 60cm away from the imaging aperture with side lobes, which can be detrimental for a multi-target scenario because one target sidelobes are as big as the second targets the main lobe.

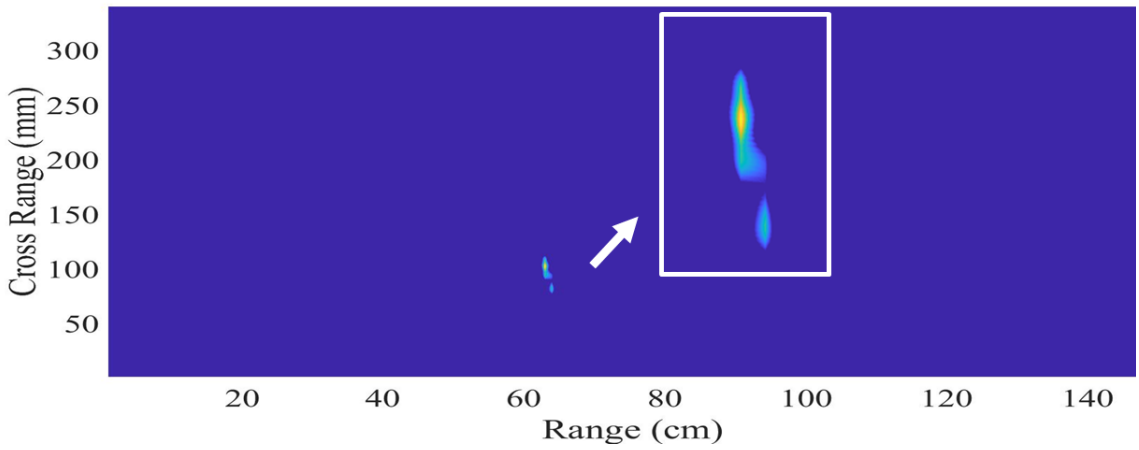

Figure 4-1 LoS reconstructed image with the target placed at 60cm away from the imaging aperture and the target extends 2cm in cross-range.

4.3 NLoS Imaging set-up and Reconstruction Steps

The concept of looking NLoS is possible if we can collect the information on the target after bouncing off of a mirror or wall. Information on the target alone is not enough because irrespective of the orientation of the wall, the target seems to be at the same range and cross-range. This means we don't have the exact orientation of the target with respect to the SAR. The perception of the exact geometry could be obtained if the orientation of the wall is known. The orientation of the wall can be used to skew the target points accordingly. Specular scattering phenomena in the microwave region from the general building materials can be used to image only the target but has information regarding the wall. Optical waves have strong, diffusive scattering phenomena that create ambiguity in the reconstructed images. In this scenario, the Terahertz region has the unique capabilities of providing a significant line of sight as well as a non-line of sight imaging. There are two

steps in the reconstruction of non-line of sight imaging, reconstruction, and localization. The back-propagation algorithm is used for the reconstruction, whereas the mirroring technique is used for the localization.

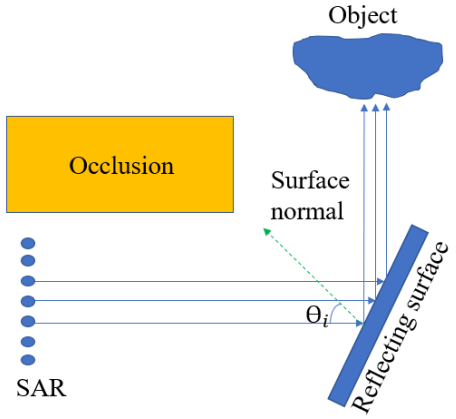

Figure 4-2 Seeing NLoS using THz imaging. By exploiting the multipath reflections of the THz signal, we identify the shape and exact position of the object scene

4.3.1 Surface Roughness of the Reflecting surface

Surface roughness depends on the geometrical properties of the wall, like the standard deviation of the roughness, incident angle, and frequency of the incident wave. The properties of the source are determined easily, but the statistical properties of the surface are tough to quantify and can be determined only through high accuracy microscopy techniques. As the surface properties are random, we also need to employ sophisticated statistical techniques for identifying scattering through a rough surface like in [38],[39]. Surface scattering at terahertz in the literature [40]-[43] proves that terahertz waves have a significant diffusive component along with a strong specular component. This property is employed for many communication strategies in [41],[43]. Hence when the terahertz waves

are bounced off of general building materials like wood, drywall, glass, epoxy [36] whose roughness is comparable to the wavelength, we can see a strong, diffusive component along with a specular component. This property of terahertz frequencies makes it a unique space in the EM spectrum which can be used for NLoS imaging

Monostatic-RCS property of the drywall surface has been used to demonstrate the property of the rough scattering. Transmitted and reflected signal are collected from the same position and in between -60° to 60° with a 2° Sampling width. RCS of drywall is compared to the specular scattering of a mirror (Copperplate) in Figure 4-3 Though the main-lobe is oriented in the same direction, the diffusion component of the drywall is 10-15dB higher the plane mirror.

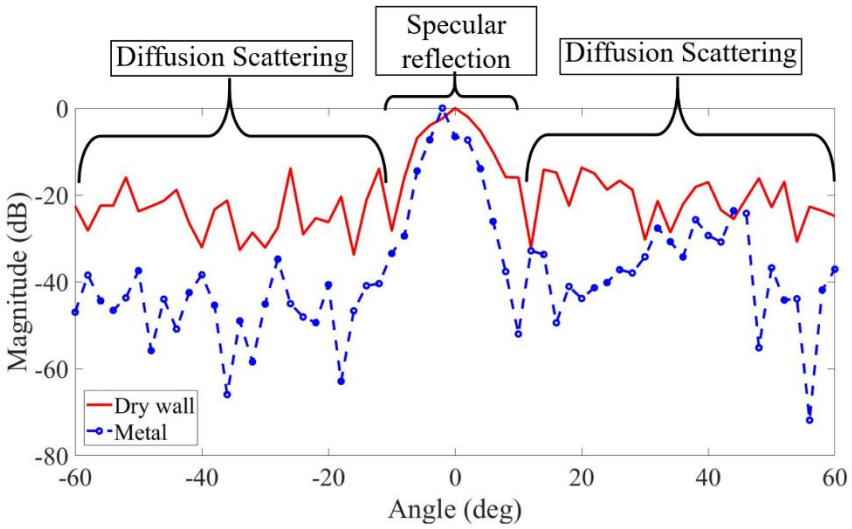

Figure 4-3 Monostatic RCS for a metallic mirror and drywall at 320 GHz. As expected, the metal exhibits stronger center lobe and lower sidelobes compared to drywall. (The metallic mirror shows increased side lobes due to scattering from objects in the lab).

4.3.2 Localization of the Raw Images in NLoS Imaging

In this task, the mirror position and orientation are used to correct the location and shape of ghost objects. Consider a simple scenario of two *non-transparent* LoS and one NLoS objects. Because of the time delay of the multireflection propagation, the NLoS object will wrongfully appear behind the LoS object. Additionally, if the LoS surface is non-planar, the NLoS object will also appear distorted. Assuming that the LoS objects are opaque, any object that appears behind the LoS object will be classified as a *ghost object*. Raw THz images can be corrected by segmenting of the entire mirror surface into smaller planar mirrors is proposed. The NLoS pixels behind every linear segment will be rotated around each individual planar mirror.

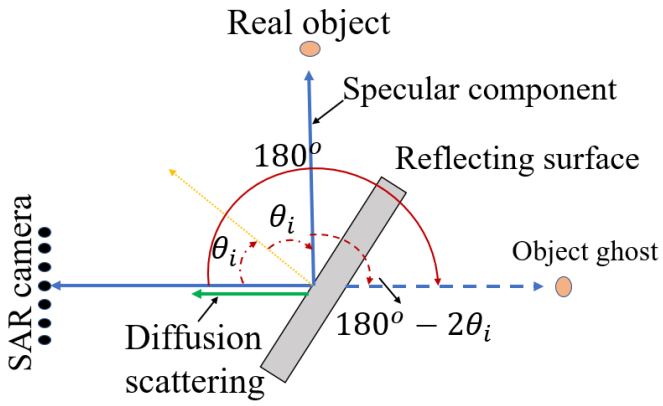

Figure 4-4 Localization or Image correction algorithm. The geometry and orientation of the reflecting surface are determined by the backscattered signals (diffuse scattering).

4.4 Single-Bounce NLoS Imaging Experiment

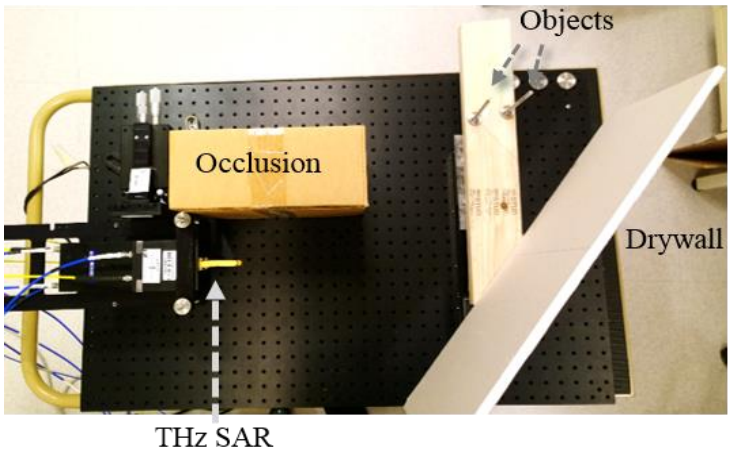

Figure 4-5 Imaging setup that is used for the implementation of non-line-of-sight imaging.

Figure 4-5 demonstrates an NLoS imaging scenario. The imaging simulation set-up uses a large piece of drywall extending from 40-60cm to capture the reflected signal from two metallic bars (6mm of diameter). SAR is implemented using (VNA) extenders, which enable the VNA to transmit the signal at THz, horn antennas, and a motorized linear stage. Here, the LOS signal from the target is directly not available to THz SAR because of the occlusion. Hence NLOS scattered signal from the drywall is the only way to form the target image. Figure 4-6 shows the raw reconstructed image formed using 12 cm SAR. Diffuse scattering is used to discern the shape of the dry-wall, and specular scattering forms the metallic bars 5 cm apart at a range of 76 cm.

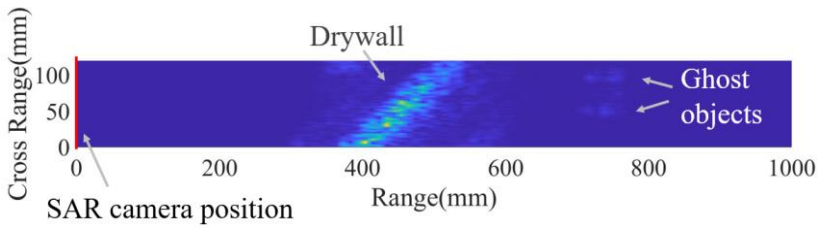

Figure 4-6 Reconstructed image of the target scene without correction. Objects appear incorrectly behind the drywall

Using the localization/mirroring technique explained in the above section, the ghost objects are placed in the corrected orientation as shown in Figure 4-7 The localized image has the exact orientation of the imaging setup in Figure 4-5 and has a cm resolution to discern the two metallic target points.

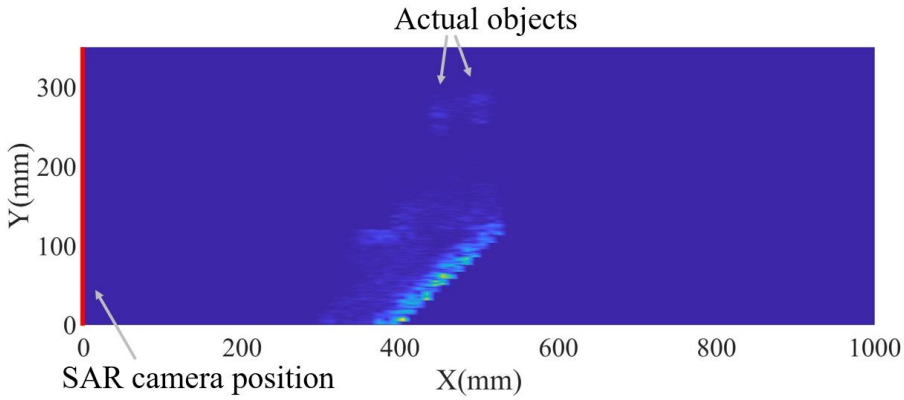

Figure 4-7 The corrected SAR image depicts all objects in the expected locations.

The next section describes a complex situation in NLoS imaging where two walls are placed at different angles with targets in front of them.

4.5 Two-wall NLoS Imaging Measurements and Results

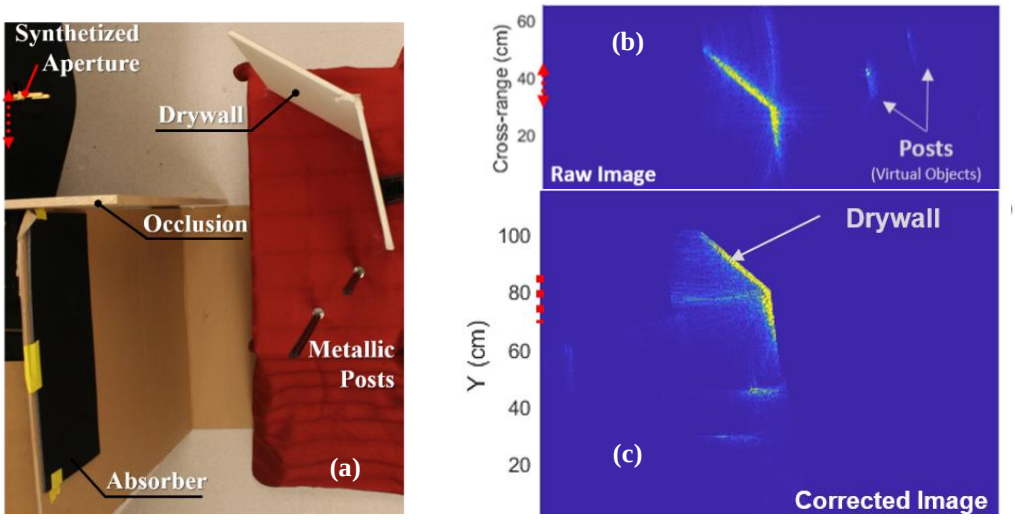

Figure 4-8 Demonstration of simple NLoS imaging with THz waves (220-325 GHz) a) Top view imaging of the experiment, b) raw image (range and cross-range), and c) corrected image accounting for drywall scattering.

Figure 4-8 (a) shows an extended imaging scenario from the above section. In the raw reconstructed image, the position of ghost objects needs to be localized to form the final image, as shown in Figure 4-8 (b). The raw reconstructed image exposes the position of ghost targets, which need to be localized to form the final image shown in Figure 4-8 (c).

Imaging experiments with two walls prove that the concept of NLoS imaging can be extended to curved walls. Where the surface is sampled into the small wall sections and localization is applied to each strip separately, forming the total image in front of the curved wall.

5 CONCLUSIONS AND FUTURE WORK

5.1 Summary and Achievements

In this work, the concept of NLoS imaging has been introduced and demonstrated for practical environments using terahertz holography. We have shown that rough surfaces exhibit significant backscattered signals due to diffuse scattering, as shown in Figure 4-3. Hense, the millimeter wave-terahertz spectrum allows imaging systems to use both diffuse and specular scattering components to enable imaging of non-line-of-sight (NLoS) objects.

Scattered wavefronts from a rough surface are converted into a discernable position of the targets using the back-propagation algorithm, as shown in Figure 4-7. Instead of depending on the return amplitude in time of flight algorithm (ToF), this technique depends on the phase of the return signal for imaging the object and solves the problem of accuracy by allocating higher bandwidth for the transmitted signal. Centimeter resolution is obtained in range and crossrange using a 15cm-long synthetic antenna aperture (1D array) and large bandwidth (100 GHz). This high spatial resolution helps in identifying metal targets that are 5 cm apart and also in identifying the orientation of a rough surface with reasonable accuracy at 76 cm distance.

Identifying the position of the target alone cannot localize the target in a complex NLoS scenario as the raw image is devoid of the orientation. We need to form the image of the reference or background and localize the target according to this image. Hence correction is achieved by rotating the target points by an angle of $180-2*\theta i$ every point behind the mirror, where θi is the angle between the synthetic aperture and the mirror. This rotation keeps both the position and orientation of target in compliance with the actual geometry.

Firstly, a simple one wall geometry with two targets that are 5cm apart is implemented. This approach though not complex enough to tackle the practical problem has the potency to prove the idea of NLoS imaging. Images of the object appear in the wrong position when compared to the actual geometry, and hence localization is employed to reflect the target points to the correct position.

Later, two walls with different orientation and targets present in front of them are used in the imaging geometry. Here each target needs to be rotated according to the orientation of the wall in front of them, as shown in Figure 4-8. This geometry adds complexity to the imaging and localization and hence paves the way for NLoS imaging to be applied for practical applications.

5.2 Applications of NLoS imaging in the Modern Age

NLoS imaging technique can aid many other fields like automation, security, and communication. Autonomous vehicles can be made more reliable with the information of the objects around the corner even before making a turn. Hence this additional information can aid the decision algorithm and avoid any sudden crashes, as shown in Figure 5-1(a). NLoS technique can be useful in potentially dangerous situations like fires, natural calamities in spotting for the people in need, as depicted in Figure 5-1(b).

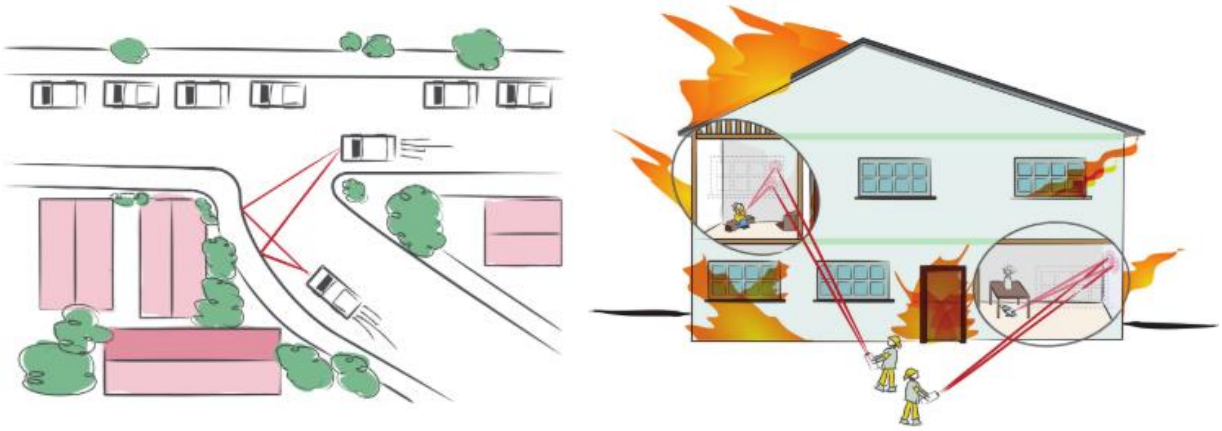

Figure 5-1 (a) NLoS imaging can help the autonomous cars for better decision making to avoid collisions (b) rescue missions can be made possible in a potentially harmful environment through this technique (Source: Available at "http://web.media.mit.edu/~raskar/cornar/ ")

Higher bandwidths achieve higher data rates, and as the world is moving toward autonomous cars, IoT (Internet of things), VR/AR (Virtual/Augmented Reality), all of which require the data rates to be in the order of several gigabits per second. Seamless communication at these rates is impossible to achieve with the available bandwidth in WAN(wide area network) bands available. Hence moving to mmWave(5G) and beyond (Terahertz) is a quintessential step in the road map to enable all these modern technologies.

For mmWave and beyond, achieving a higher throughput might be inefficient with the concurrent techniques available because of the higher path loss, lack of line-of-sight, and complexity in the channel models at higher frequencies. Hence, there is a need for the latest techniques that can exploit the mmWave band. One such is presented below using the NLoS imaging technique.

In current mmW wireless communications, the system can determine the time-of-arrival (ToA) and angle-of-arrival (AoA) with the use of pilot signals, but unless the user is in LoS, localization becomes challenging without prior knowledge of the environment geometry. NLoS imaging can aid this area by providing information about the environment geometry like the orientation of walls. Most of the practical building materials like drywall, wood act as a mirror for terahertz frequencies [40],[43]. Hence this NLoS image can be used to localize the user position, thus providing a way for better channel parameter estimation and link establishment. The details above concept are given in [44].

Hence making NLoS robust and practically applicable can aid advancements in other fields like described above. The next section presents a couple of enhancement ideas that could be implemented for making NLoS Imaging more suitable for practical application scenarios.

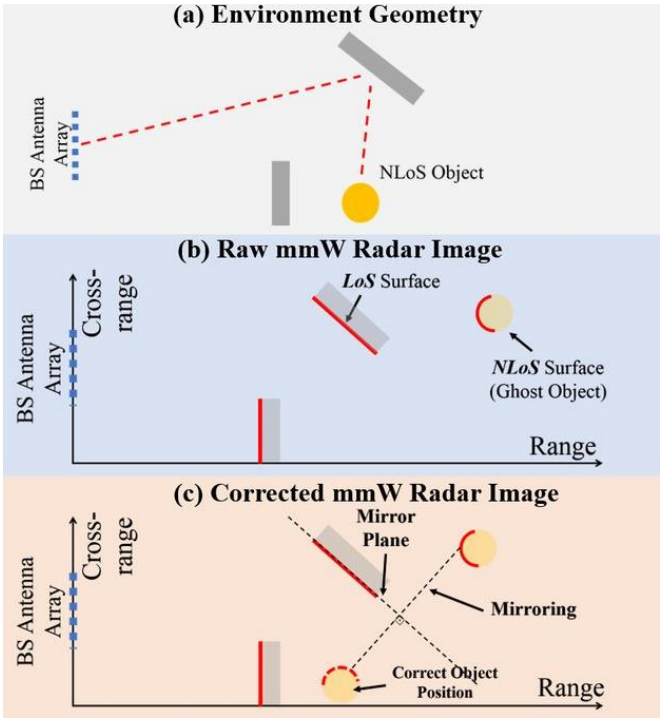

Figure 5-2 NLoS technique is employed for identification of user position and orientation from the base station antenna array [43]

5.3 Future Work and Improvements for NLoS Technique :

Despite the achievements in NLoS imaging, Several improvements and challenges have been observed to improve this technique. Improving the reliability of NLoS imaging techniques requires work in the areas of both imaging and localization.

- Currently, the employed approach has a manually chosen reference line for localizing the objects; this approach is prone to human error. This error can be propagated as a wrong target orientation, shown in Figure 5-3 below. The reference line can be chosen based on the signal strength in the total wall image area or based

on the speckle identification in the wall. Advanced nonlinear algorithms can be employed for better identification of the orientation of the wall.

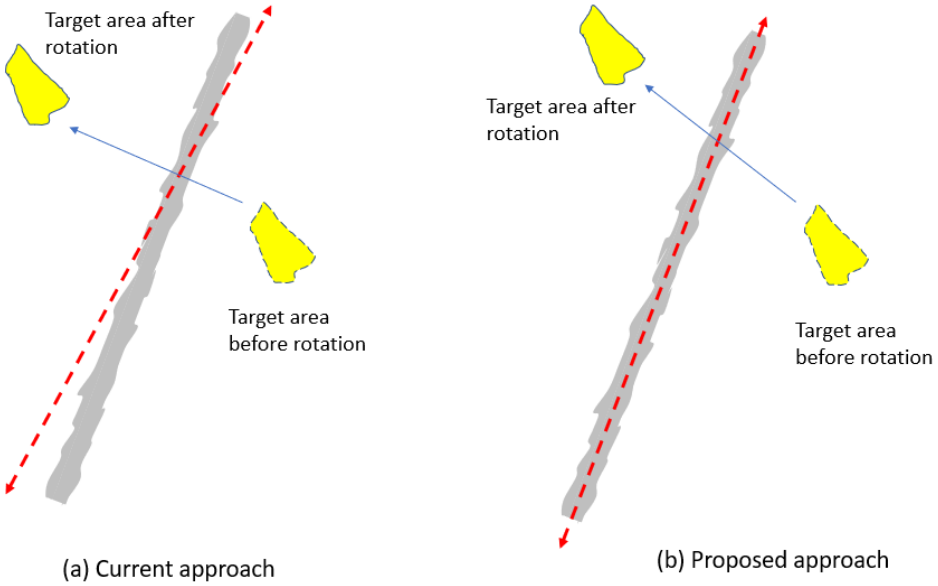

Figure 5-3 (a) Erroneous reference chosen reference line resulted in a wrong orientation of the target (b) automatic reference line can result in the proper orientation of the localized target points

- The practical geometries have curved walls and random geometries for reflecting the incident waves, and this curvature can be approximated using multiple straight walls, as shown below in fig 5-5. Thus, NLoS imaging can be implemented for each straight wall separately by mirroring the objects in front of them. This technique can make NLoS imaging suitable for the practical imaging geometries

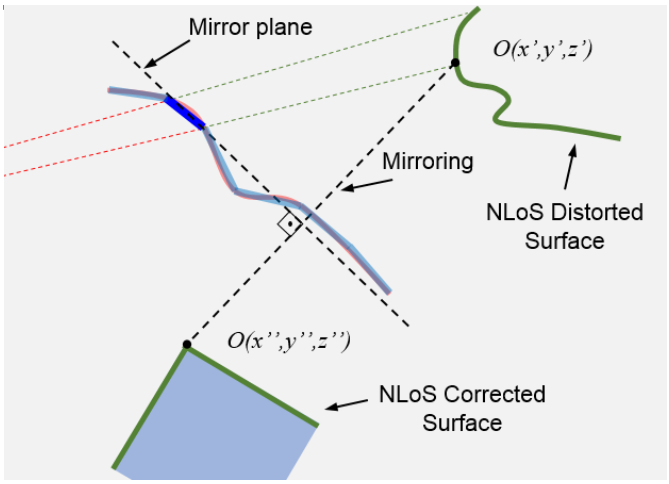

Figure 5-4 Curved reflecting surface has been divided into multiple straight walls, and thus each section can be treated as a separate wall for proper orientation of the target

- Multi-static imaging approach could improve the reliability in identifying the ghost images, which is not possible for a mono-static approach due to a single point of view and the limited *k*-space. Intelligent multi-static could also be employed to improve the image acquisition time, which could make the NLoS technique a real-time technique.

REFERENCES

[1] A. Kirmani, T.Hutchison, J.Davis, and R.Raskar, “Looking Around the Corner Using Ultrafast Transient Imaging” Int J Comput Vis, vol no 95, pp:13–28, June 2011.

[2] A.Velten, T. Willwacher, O.Gupta ,A.Veeraraghavan, M. G. Bawendi, R.Raskar, “Recovering three-Dimensional shape around a corner using ultrafast time-of-flight Imaging”, Nature Communications, 3:745, Mar 2011.

[3] Gabor (1948) ‘A new microscopic principle’,*Nature*, 161, p 777 – 778.

[4] Lippmann’s and Gabor’s Revolutionary Approach to Imaging by Klaus Biedermann. Available:https://www.nobelprize.org/prizes/uncategorized/lippmanns-and-gabors-revolutionary-approach-to-imaging-2/

[5] I. Skolnik, M. (1980). Introduction to radar systems /2nd edition/. New York, McGraw Hill Book Co., 1980.

[6] Richards, Mark & Scheer, J.A. & Holm, W.A.(2010). Principles of modern radar: Basic principles.

[7] Mehrdad Soumekh. 1994. Fourier Array Imaging. Prentice-Hall, Inc., Upper Saddle River, NJ, USA

[8] Carrara, Walter G, Ron S. Goodman, and Ronald M. Majewski. Spotlight Synthetic Aperture Radar: Signal Processing Algorithms. Boston: Artech House, 1995. Print.

[9] E. Zaugg, “Generalized Image Formation for Pulsed and LFM-CW Synthetic Aperture
Radar,” Ph.D. dissertation, Brigham Young University, 2010.

[10] Ahmed, Sherif. (2015). Electronic Microwave Imaging with Planar Multistatic Arrays.

[11] M.Younis, Digital Beam-Forming for High Resolution Wide Swath Real and Synthetic Aperture Radar," Ph.D. dissertation, Universit¨at Karlsruhe (TH), 2004.

[12] . Griffiths, N.Willis and Klein Heidelberg,”The First Modern Bistatic Radar System", IEEE Transactions on Aerospace and Electronic Systems, vol. 46, no. 4, pp. 1571-1588, Oct. 2010

[13] G. Yates, A. Horne, A. Blake, and R. Middleton, "Bistatic SAR Image Formation", IEE Proceedings - Radar, Sonar and Navigation, vol. 153, no. 3, pp. 208-213, 2006.

[14] A G Davies et al., “The Development of Terahertz Sources and their Applications,” Physics in Medicine and Biology, Oct 17, 2002

[15] D. Joye, Colin, M. Cook, Alan, P. Calame, Jeffrey, Abe, David, N. Vlasov, Alexander, Chernyavskiy, Igor, T. Nguyen, Khanh, L. Wright, Edward,, E. Pershing, Dean, Kimura, T, Hyttinen, Mark, and Levush, Baruch. "Demonstration of a High Power, Wideband 220-GHz Traveling Wave Amplifier Fabricated by UV-LIGA," in IEEE Transactions on Electron Devices, vol. 61, no. 6, pp. 1672-1678, June 2014.

[16] X. Mei, W. Yoshida, M. Lange, J. Lee, J. Zhou, P. Liu, K. Leong, A. Zamora, J. Padilla, S. Sarkozy, R. Lai, and W. R. Deal, "First Demonstration of Amplification at 1 THz Using 25-nm InP High Electron Mobility Transistor Process," in IEEE Electron Device Letters, vol. 36, no. 4, pp. 327-329, April 2015.

[17] M. A. Patrick, J.A.Holt,C.D. Joye, and F.C.De Lucia, “Elimination of speckle and target orientation requirements in millimeter-wave active imaging by modulated multimode mixing illumination,” J. Opt. Soc. Am. A 29, 2643–2656 (2012)

[18] M. A. Patrick, J. A. Holt, C. D. Joye, and F. C. De Lucia, "Range resolved mode mixing in a large volume for the mitigation of speckle and strategic target orientation requirements in active millimeter-wave imaging," J. Opt. Soc. Am. A 32, 637-646 (2015).

[19] Freund, Isaac and Rosenbluh, Michael and Feng, Shechao, “Memory Effects in Propagation of Optical Waves through Disordered Media, ” in Phys. Rev. Lett., vol.61, no.20, pp. 2328-2331, nov.1988.

[20] Bertolotti Jacopo, van Putten, Elbert G., Blum Christian, Lagendijk Ad, Vos Willem L., Mosk Allard P.,” Non-invasive imaging through opaque scattering layers,” in Nature, nov 2012.

[21] Jour, Katz Ori,Small Eran,Silberberg Yaron,” Looking around corners and through thin turbid layers in real time with scattered incoherent light,” in Nature Photonics, vol. 6, July 2012

[22] M. O’Toole, D. B. Lindell, and G. Wetzstein, “Confocal non-line-of-sight imaging based on the light-cone transform,” Nature volume 555, pages 338–341 (15 March 2018).

[23] F. Xu, G. Shulkind, C. Thrampoulidis, J. H. Shapiro, A. Torralba, F. N. C. Wong, and G. W. Wornell, "Revealing hidden scenes by photon-efficient occlusion-based opportunistic active imaging," Opt. Express 26, 9945-9962 (2018)

[24] K. P. H. Thai *et al*., "Around-the-corner radar: Detection and localization of a target in non-line of sight," *2017 IEEE Radar Conference (RadarConf)*, Seattle, WA, 2017, pp. 0842-0847.

[25] R. Zetik, M. Eschrich, S. Jovanoska and R. S. Thoma, "Looking behind a corner using multipath-exploiting UWB radar," in *IEEE Transactions on Aerospace and Electronic Systems*, vol. 51, no. 3, pp. 1916-1926, July 2015.

[26] O. Rabaste, E. Colin-Koeniguer, D. Poullin, A. Cheraly, J. F. Pétex, and H. K. Phan, "Around-the-corner radar: detection of a human being in non-line of sight," in IET Radar, Sonar & Navigation, vol. 9, no. 6, pp. 660-668, 7 2015.

[27] A. Sume, M. Gustafsson, M. Herberthson, A. Jannis, S. Nilsson, and J. Rahm, "Radar Detection of Moving Targets Behind Corners," in IEEE Transactions on Geoscience and Remote Sensing, vol. 49, no. 6, pp. 2259-2267, June 2011.

[28] S. K. Doddalla and G. C. Trichopoulos, "Non-Line-of-Sight Terahertz Imaging from a Single Viewpoint," 2018 IEEE MTT-S International Microwave Symposium, Philadelphia, PA, June 10-15, 2018.

[29] Goodman, Joseph & H. Huntley, W & W. Jackson, D & Lehmann, M. (1966). Wavefront-reconstruction imaging through random media. Applied Physics Letters. 8. 311 - 313. 10.1063/1.1754453.

[30] H. Kogelnik and K. S. Pennington, "Holographic Imaging Through a Random Medium," J. Opt. Soc. Am. 58, 273-274 (1968)

[31] M. Soumekh, Synthetic aperture radar signal processing with MATLAB Algorithms. New York: Wiley, 1999, vol. 7.

[32] D. M. Sheen, D. L. McMakin and T. E. Hall, "Three-dimensional millimeter-wave imaging for concealed weapon detection," in IEEE Transactions on Microwave Theory and Techniques, vol. 49, no. 9, pp. 1581-1592, Sep 2001.

[33] Guo, Qijia & Chang, Tianying & Geng, Guoshuai & Jia, Chengyan & Cui, Hong-Liang. (2016). A High Precision Terahertz Wave Image Reconstruction Algorithm. Sensors. 16. 10.3390/s16071139.

[34] S. S. Ahmed, A. Schiessl, and L. P. Schmidt, "A Novel Fully Electronic Active Real-Time Imager Based on a Planar Multistatic Sparse Array," in IEEE Transactions on Microwave Theory and Techniques, vol. 59, no. 12, pp. 3567-3576, Dec. 2011.

[35] FEKO 14.1 Stellenbosch, South Africa, E. S. Systems. Available: http://www.feko.info

[36] The MathWorks Inc., \MATLAB," 2018

[37] "Virginia diodes inc." [Online]. Available: https://www.vadiodes.com/en/

[38] P. A. Beckmann and A. Spizzichino, The Scattering of Electromagnetic Waves From Rough Surfaces, 2 ed. Norwood, MA, USA: Artech House, 1987, p. 503.

[39] A. G. Voronovich, Wave Scattering From Rough Surfaces, 2nd ed. (Springer Series on Wave Phenomena). Berlin, Germany: Springer-Verlag, 1999, p. 234.

[40] E. N. Grossman, N. Popovic, R. A. Chamberlin, J. Gordon, and D. Novotny, "Submillimeter Wavelength Scattering from Random Rough Surfaces," in IEEE Transactions on Terahertz Science and Technology, vol. 7, no. 5, pp. 546-562, Sept. 2017.

[41] R. Piesiewicz, C. Jansen, D. Mittleman, T. Kleine-Ostmann, M. Koch, and T. Kurner, "Scattering Analysis for the Modeling of THz Communication Systems," in IEEE Transactions on Antennas and Propagation, vol. 55, no. 11, pp. 3002-3009, Nov. 2007.

[42] C. Jansen, R. Piesiewicz, D. Mittleman, T. Kurner, and M. Koch, "The Impact of Reflections From Stratified Building Materials on the Wave Propagation in Future Indoor Terahertz Communication Systems," in IEEE Transactions on Antennas and Propagation, vol. 56, no. 5, pp. 1413-1419, May 2008.

[43] C. Jansen, S. Priebe, C. Moller, M. Jacob, H. Dierke, M. Koch, and T. Kurner, "Diffuse Scattering From Rough Surfaces in THz Communication Channels," in IEEE Transactions on Terahertz Science and Technology, vol. 1, no. 2, pp. 462-472, Nov. 2011.

[44] Aladsani, Mohammed & Alkhateeb, Ahmed & Trichopoulos, Georgios. (2019). Leveraging mmWave Imaging and Communications for Simultaneous Localization and Mapping. 4539-4543. 10.1109/ICASSP.2019.8682741.